Energy Conversion and Management: X 23 (2024) 100598

Contents lists available at ScienceDirect

Energy Conversion and Management: X

journal homepage: www.sciencedirect.com/journal/energy-conversion-and-management-x

Optimal day-ahead active and reactive power management for microgrids with high penetration of renewables

Matteo Fresia [a,*], Laura Bordo [b], Federico Delfino [a], Stefano Bracco [a]

[a] Department of Electrical, Electronic, Telecommunications Engineering and Naval Architecture – University of Genoa, via Opera Pia 11a, 16145 Genova, Italy
[b] RINA Consulting S.p.A., via Cecchi 6, Genova, Italy

ARTICLE INFO

Keywords:
Microgrid
Energy management system
Optimization
Reactive power management
Curtailment
Solar energy
Wind energy

ABSTRACT

In recent years, efforts have been made to increase the proportion of electricity demand met by Renewable Energy Sources (RESs). Distributed Energy Resources (DERs) play a crucial role in this frame, particularly in Microgrids (MGs) where DERs and clusters of loads are interconnected. This paper presents an Energy Management System (EMS) developed for a low-voltage MG installed in Italy, connecting Photovoltaic (PV) units, a Wind Turbine (WT), a Battery Energy Storage System (BESS), a Combined Heat and Power (CHP) unit and loads: the EMS aims to optimize the day-ahead scheduling of the MG, considering both economic and power quality criteria. The mathematical model incorporates the capability curves of the inverters connected to DERs and allows for curtailment of PV and WT units, with curtailment costs assessed using the Levelized Cost of Electricity (LCOE). Penalties for the absorption of reactive power from the external network are considered and evaluated in accordance with the current regulatory framework. Optimal Power Flow (OPF) equations are integrated into the EMS model, too. A preliminary analysis, carried out on a simplified MG, evaluates the impact of linearizing the DERs capability curves and OPF equations on the EMS's outcomes. Finally, a sensitivity analysis evaluates the impact of different operational constraints and of different objective function formulations on the operation of the MG, discussing key energy and economic results.

1. Introduction

In recent years, there has been a growing concern over the environmental impact of traditional electricity generation from fossil fuels. Renewable Energy Sources (RESs) have been widely identified as the main solution to this issue. In the last decades, the European Union (EU) has continuously improved its objectives in climate change fighting. Recently, the "Fit for 55" package has been enacted [1]: among its several goals, it aims to reduce greenhouse-gas emissions by at least 55% by 2030 (compared to 1990 levels) and to increase the market share of renewable energy up to 40%. Besides, the share of renewable energy consumed in buildings has to reach 49%, with a step-increase of that share also in industry and heating/cooling systems.

RESs will play a fundamental role in ensuring this transition, providing sustainable and green energy [2]. Nevertheless, RESs like Wind Turbines (WTs) and Photovoltaic (PV) power plants are inherently affected by the unpredictability of the physical source (solar and wind), meaning that they may not be able to instantaneously follow the variation of the load demand [3]. Besides, being connected to the network via inverters, they may not be able to provide inertial response and primary frequency support, if not properly controlled.

In order to overcome the unpredictability issue, energy storage systems like Battery Energy Storage Systems (BESSs) are frequently installed, acting as buffers, dampening the oscillation in the renewable energy production by ensuring a steady supply of electricity to the grid [4,5]. This stabilization effect is crucial for keeping the grid stable and reliable, allowing a greater amount of RES-produced energy to be integrated into the existing power infrastructure [6], easing the matching between generation and demand. If properly controlled, RESs and BESSs are able to participate in frequency support to the network, providing synthetic inertial responses and participating in primary frequency regulation, in accordance with grid codes [7].

The increasing exploitation of RESs, coupled with advancements in Distributed Generation (DG) technologies, has led to the emergence of Microgrids (MGs) as an efficient and sustainable solution for power generation and distribution. An MG can be defined as a localized group of interconnected loads and Distributed Energy Resources (DERs) able to operate either in parallel with the main grid or autonomously during an outage [8]. DERs units are typically RESs, high-efficiency cogeneration

* Corresponding author.
E-mail address: matteo.fresia@edu.unige.it (M. Fresia).

https://doi.org/10.1016/j.ecmx.2024.100598
Received 19 February 2024; Received in revised form 19 April 2024; Accepted 20 April 2024
Available online 23 April 2024

Nomenclature

Acronym

AC	Alternating Current
BESS	Battery Energy Storage System
CHP	Combined Heat and Power
DER	Distributed Energy Resource
EMS	Energy Management System
EV	Electric Vehicle
LCOE	Levelized Cost of Electricity
LF	Load Flow
MG	Microgrid
MILP	Mixed-Integer Linear Programming
MINLP	Mixed-Integer Non Linear Programming
OPF	Optimal Power Flow
PV	Photovoltaic
RES	Renewable Energy Source
WT	Wind Turbine

Symbol

B	Number of busses [-]
C	Capacity [kWh]
E	Energy [kWh]
N	Number of cycles
S	Base apparent power [kVA]
T	Number of time intervals [-]
W,w,y	Binary variable [-]
a	Apparent power [p.u.]
l	Length [km]
p	Active power [p.u.]
q	Reactive power [p.u.]
r	Resistance [p.u]
soc	State of Charge [-]
u	Voltage deviation [p.u.]
v	Voltage [p.u.]
x	Reactance [p.u.]
Δ	Time interval duration [h]
α	Capability curve coefficient [-]
γ, μ	Weight coefficient [-]
δ	Angle [rad]
η	Efficiency [-]
ς	Ramp rate [-]
ρ	Penalty [€/kVARh]
σ	Price[€/kWh]
τ	Curtailment cost [€/kWh]

Superscript

L	Load
T	Transformer
Av	Available
Ch	Charging
Curt	Curtailed
Dch	discharging
Q	Reactive
St	Storage

Subscript

b,k	bus
t	time

units (small-medium size) and BESSs. All these sources operate as a single controllable system that provides both power and heat to its local area. Whenever a Combined Heat and Power (CHP) unit is installed in the MG, the electrical and thermal infrastructures are intrinsically coupled. Compared to traditional distribution systems, MGs offer a greater flexibility in controlling DER units [9], ensuring an increased reliability of electrical services, the ability to dispatch local power and an enhanced power supply efficiency, through strategically located CHP units [10,11].

Therefore, MGs are based on complex multi-energy vector systems that need to be optimally scheduled and operated in order to fully exploit their peculiarities: for this purpose, Energy Management Systems (EMSs) are required, in order to find the optimal planning of the DERs, optimizing the power flows between each unit, both in islanded and grid-connected mode, according to economic, environmental or technical criteria [12]. Besides, reactive power provision and voltage support are further challenges that will involve inverter-based DERs: for this reason, inverters' capability curves will have to be considered by EMS, in order to model the capability of these sources to provide inductive or capacitive reactive power [13].

Several examples of EMSs are present in literature, dealing with Optimal Power Flow (OPF) constraints. The main constraints are i) active power constraints for generation, ii) reactive power constraints about the maximum reactive power that can be injected into the power system, iii) voltage amplitude and voltage phase constraints to ensure reliable operations of the system and iv) current constraints [14].

An EMS for a urban MG is formalized in [15] and furtherly developed in [16]. In these papers, the analysed MG is connected to a local distribution network and is formed by interconnected loads (both controllable and non-controllable), RES generation and a centralized BESS. The EMS is based on a predictive control management, which relies on day ahead OPF analysis, in order to optimize the energy flows and provide ancillary services to the external network.

An EMS for the optimal operation of a grid-connected building equipped with renewable generation and a fleet of Electric Vehicles (EVs) is presented in [17] and furtherly developed in [18]. The energy flows between the different units, the building and the network are optimized in order to minimize the operational costs, taking into account both active and reactive energy exchanges and RES curtailment costs.

Two EMSs for islanded hybrid MGs are compared in [19]. The proposed strategies enable the real time operation of the hybrid MG, always guaranteeing its correct operation. The first EMS strategy works by assigning a priority order, reflecting the dispatchment priority of the energy sources installed in the MG, with the aim of minimizing the operating costs. The second strategy is based on a centralized optimization architecture: the aim is to minimize the marginal costs for each generation unit. Different scenarios are tested to help the power system operator obtain the optimal operation strategies of the MG.

An optimal energy management model is presented in [20]. The facility is composed of a PV unit, a diesel generator and a BESS, for the supply of some critical loads in off-grid applications.

A further formulation of EMS is proposed in [21], dealing with a hybrid MG, equipped with PV and WT units, a BESS and a connection to the external grid. The EMS aims to reduce the total energy cost and the storage utilization. The authors introduced a coefficient within the mathematical structure of the EMS, linking the amount of power discharged from the BESS to the electricity price from the main grid.

A two-level optimization EMS applied to a multi-energy scenario considering electricity and hydrogen as energy vectors is studied in [22]. The designed EMS takes into consideration an objective function related to economic profitability and constraints referred to the availability of the sources and storage solutions, their reliability and the costs. One of the main contributions of the paper is to compare the possible ways of exploitation of the energy available in an industrial MG.

In [23], an approach for the development of an EMS is proposed, optimizing both active and reactive power flows in a smart MG composed of residential loads, a BESS, a PV system, a micro gas turbine and a connection to the main power grid. The EMS objective is double: minimizing the cost of the generated power and reduce the CO_2 emissions of the gas turbine.

Reference [24] proposes a formulation of the optimal design and operation of a local energy community integrating electric mobility service, RESs and a BESS. The energy community exploits a local MG to exchange electricity between the participants.

EMSs for the optimal scheduling of university MGs are proposed in [25] for islanded MG operations, in [26] with a heuristic approach and in [27–29] for a facility located in Italy with renewable generation from PV plant, geothermal heat pump and EV integration.

An approach for the optimal management of multi-generation energy systems is proposed in [30], with a focus on the minimization of primary energy consumption and operating costs.

Nevertheless, all the aforementioned studies are linked by the application of a single busbar model to the studied MGs: this is a main drawback, since single busbar model neglects all the voltage phenomena that may occur in a multi busbar network, disregarding the application of OPF equations and of voltage-related analyses. In fact, voltage drops actually occurring on MG cables are neglected and the optimization of active and reactive power flows to limit voltage deviation at busses is not proposed.

An example of EMS including OPF equations is presented in [31], considering a multi busbar model of a power network to which conventional generation sources and RESs are connected. The authors propose different formulations of the objective function, considering either alternatively or together the minimisation of operating cost, of gas emissions, of power losses and of voltage deviations at the busses.

In [32], different dispatching strategies for a multi busbar islanded MG located in Australia are proposed and tested, in order to optimize greenhouse gas emissions and the levelized cost of energy.

The authors of [33] propose an optimal operation strategy for a droop-controlled islanded MG, composed of six busses to which PV plants, DERs and loads are connected, considering complete OPF equations.

Similar application of full OPF equations can be found in [34], where a strategy for the optimal management of electrical and thermal resources is proposed, in presence of heat pumps, CHP units, renewable generation and a BESS.

Nevertheless, the authors of the aforementioned studies either did not provide information about the structure of the employed OPF equations (see [32]) or did not deeply discuss the computational effort required by a non-linear model (see [31,33;34]), like the classical OPF model, and consequently not delivering an analysis about the possible computational benefits that might derive from a linearisation of the model. Besides, voltage optimization through the management of active and reactive power flows is again not considered and discussed, partially not exploiting the introduction of OPF equations and of multi busbar models.

Starting from this state of art, the present paper proposes an EMS that ensures the optimal operation and scheduling of a polygenerative MG, modelled as a multi busbar grid, in order to minimize both economic and technical indicators (e.g. energy purchase costs, energy sale revenues, voltage deviation). The MG is connected to the medium voltage distribution network and is equipped with WTs, PV units, BESSs, a CHP unit and loads. Cables have been included in the electrical model of the network, with proper values of resistance and reactance, thus taking into account Load Flow (LF) equations. Capability curves, compliant with the current grid codes, have been modelled within the EMS to optimally manage reactive power flows, as well as via the introduction of costs related to RES curtailment and reactive power absorption from the external network. By running the EMS over 24 hours with a time resolution of 10 minutes, the optimal operation of the MG has been studied to evaluate the impact of different objective function formulations, taking into account economic and voltage indicators.

Preliminarily to the analysis of the "full" MG, a study was conducted on a simplified version of the MG in order to gain some useful insights to be used for the development of the final EMS, like the possibility of linearising LF equations, in order to gain useful computational and resolution benefits.

The novelty of the present work is the coupled optimization of active and reactive power flows, unlike other previous studies that propose a separate dispatchment of the two quantities (see [35,36]). Besides, another highlight of the present paper is the modelling of the MG as a multi busbar network, instead of the single busbar model commonly applied in literature. In addition, this paper preliminarily delivers an assessment of the linearisation of a model that in principle is nonlinear: in other words, the present paper analyses the deviation of the results obtained with linearised OPF equations from the ones obtained with full (nonlinear) OPF equations.

Summarizing, the main contributions of the present paper are:

- Detailed modelling of CHP units, BESSs and RES plants in terms of active and reactive power, with the possibility to apply RES curtailment;
- Modelling of BESS charge and discharge phases taking into account ramp-up and ramp-down constraints and maximum number of cycles, in order to limit the aging of batteries and to represent the real-world behaviour of the system;
- Comparison of full OPF equations with linearised OPF equations, providing a sensitivity analysis to assess the impact of the linearization on the results and on the computational effort and to define the range of validity of the linearised approach as a function of the MG dimension;
- Evaluation of the impact of RES penetration and BESS availability on bus voltages through a sensitivity analysis;
- Definition of a complex objective function, considering operating net costs, related to the power exchange with the public network and to curtailment, reactive power dispatching priority for DER inverters and bus voltage deviation from rated values.

This paper is structured as follows: Section 2 presents a detailed description of the optimization mathematical model that has been developed; Section 3 describes the technical input data that have been considered and the results, for both the simplified MG and the "full" MG, providing also sensitivity analyses considering increased penetration of RESs and the service outage of the BESS, to assess the impact on bus voltages. Finally, some concluding remarks, together with a discussion of possible future developments, are presented in Section 4.

2. Methodology

The EMS is based on a mathematical model characterized by a time horizon equal to 1 day split into T time intervals, each one having a duration of Δ. This section describes the main constraints used to model each technology and reports the adopted objective function, also highlighting input data and parameters. The EMS, of day-ahead type, can be applied to daily operate an AC-MG with RES power plants, storage systems, CHP units and loads. It is assumed that the MG has a ring configuration with B busses and presents a unique point of common coupling with the medium voltage distribution network. Two version of the EMS are proposed, a first one based on a Mixed-Integer Linear Programming (MILP) model with linearized LF equations and a second one based on a Mixed-Integer Non-Linear Programming (MINLP) model with full LF equations. Powers and voltages are given "per unit" in the formulae, unless otherwise stated, and the assumed base power is called S^{base}.

2.1. RES model

The model assumes that at most one RES plant (i.e. PV plant, small WT, small hydro plant, etc.) can be connected to each bus b ($b = 1 \ldots B$). The main technical specification that characterizes the installation is the rated apparent power of the inverter associated with the plant, indicated by a_b^{RES}. On the other hand, $p_{b,t}^{RES,av}$ indicates the average available active power that can be produced by the plant in time interval t ($t = 1 \ldots T$). The decision variables which describe the operation of the plant within the optimization model can be defined as follows:

- $q_{b,t}^{RES,out}$: supplied inductive reactive power;
- $q_{b,t}^{RES,in}$: absorbed inductive reactive power;
- $y_{b,t}^{RES,out}$: binary variable equal to 1 when the plant provides inductive reactive power to the MG;
- $y_{b,t}^{RES,in}$: binary variable equal to 1 when the plant absorbs inductive reactive power from the MG
- $p_{b,t}^{RES}$: active power output;
- $p_{b,t}^{RES,curt}$: curtailed active power.

A rectangular capability curve is introduced to model the limits of the active and reactive power that the inverter can exchange, as prescribed by the Italian technical standards CEI-021 [37] for inverters connected to low voltage networks. An example of rectangular capability curve is provided in Fig. 1.

Constraints (1) are used to define the permissible active power values whereas constraints (2) and (3) refer to limits on the inductive reactive power supplied and absorbed, respectively. The coefficient $\alpha_b^{RES,q}$ is typically provided by the inverter manufacturer and usually refers to technical standards.

$$0 \leq p_{b,t}^{RES} \leq a_b^{RES} \quad \forall t = 1 \ldots T, \forall b = 1 \ldots B \tag{1}$$

$$0 \leq q_{b,t}^{RES,out} \leq \alpha_b^{RES,q} \cdot a_b^{RES} \cdot y_{b,t}^{RES,out} \quad \forall t = 1 \ldots T, \forall b = 1 \ldots B \tag{2}$$

$$0 \leq q_{b,t}^{RES,in} \leq \alpha_b^{RES,q} \cdot a_b^{RES} \cdot y_{b,t}^{RES,in} \quad \forall t = 1 \ldots T, \forall b = 1 \ldots B \tag{3}$$

Constraints (4) ensure that the plant cannot simultaneously supply and absorb inductive reactive power, whereas constraints (5) and (6) permit to model curtailment, if the RES production has to be cut to keep the system safe.

$$y_{b,t}^{RES,out} + y_{b,t}^{RES,in} \leq 1 \quad \forall t = 1 \ldots T, \forall b = 1 \ldots B \tag{4}$$

$$p_{b,t}^{RES,av} - p_{b,t}^{RES} - p_{b,t}^{RES,curt} = 0 \quad \forall t = 1 \ldots T, \forall b = 1 \ldots B \tag{5}$$

$$p_{b,t}^{RES,curt} \geq 0 \quad \forall t = 1 \ldots T, \forall b = 1 \ldots B \tag{6}$$

2.2. Grid model

The MG is connected to the medium voltage distribution network via a transformer having a rated apparent power equal to a^T and modelled by a squared capability curve in the MILP model and by a circular capability curve in the MINLP model. The decision variables which describe the power exchanged at time t between the MG and the distribution network are:

- p_t^{buy}: active power withdrawn from the network;
- p_t^{sell}: active power injected into the network;
- w_t^{buy}: binary variable equal to 1 when the MG is buying electricity;
- w_t^{sell}: binary variable equal to 1 when the MG is selling electricity;
- q_t^{buy}: inductive reactive power withdrawn from the network;
- q_t^{sell}: inductive reactive power injected into the network;
- y_t^{buy}: binary variable equal to 1 when the MG is absorbing inductive reactive power from the network;
- y_t^{sell}: binary variable equal to 1 when the MG is injecting inductive reactive power into the network.

In the MILP model constraints from (7) to (9) define limits for active power whereas constraints from (10) to (12) set reactive power limits. In

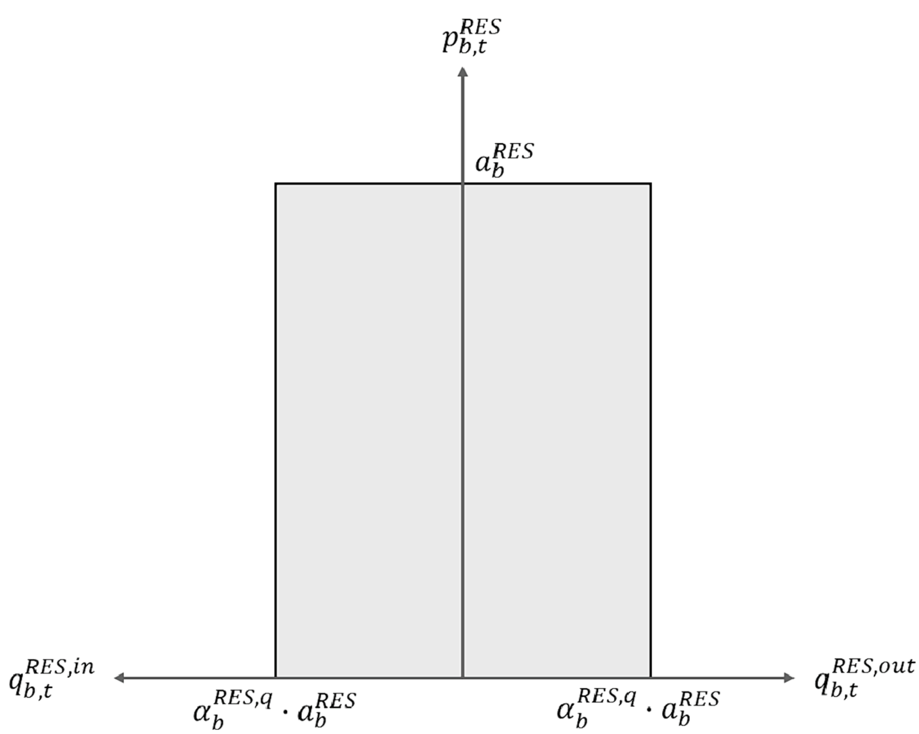

Fig. 1. Inverter capability curve for RES plants.

particular, constraint (9) prevents from buying and selling active energy at the same time, while constraint (12) does the same for reactive power.

$$0 \le p_t^{buy} \le a^T \cdot w_t^{buy} \quad \forall t = 1 \dots T \tag{7}$$

$$0 \le p_t^{sell} \le a^T \cdot w_t^{sell} \quad \forall t = 1 \dots T \tag{8}$$

$$w_t^{buy} + w_t^{sell} \le 1 \quad \forall t = 1 \dots T \tag{9}$$

$$0 \le q_t^{buy} \le a^T \cdot y_t^{buy} \quad \forall t = 1 \dots T \tag{10}$$

$$0 \le q_t^{sell} \le a^T \cdot y_t^{sell} \quad \forall t = 1 \dots T \tag{11}$$

$$y_t^{buy} + y_t^{sell} \le 1 \quad \forall t = 1 \dots T \tag{12}$$

In the MINLP model, constraints from (7) to (12) continue to apply but it is also necessary to include constraint (13) that defines the circular capability curve of the transformer, as presented in [18].

$$\left(p_t^{buy} + p_t^{sell}\right)^2 + \left(q_t^{buy} + q_t^{sell}\right)^2 \le \left(a^T\right)^2 \quad \forall t = 1 \dots T \tag{13}$$

2.3. CHP model

The EMS assumes that each CHP unit in the MG operates in thermal priority mode: therefore, the operation of the CHP unit is primarily defined in order to satisfy the thermal load. The electrical active power produced ($p_{b,t}^{CHP}$) follows accordingly, in accordance with the heat/power curve of the CHP unit: therefore, $p_{b,t}^{CHP}$ is assumed as input to the EMS, as the presented EMS does not model the thermal part of the MG. Consequently, the decision variables describing the operation at time t of the CHP unit connected to bus b are:

- $q_{b,t}^{CHP,out}$: supplied inductive reactive power;
- $q_{b,t}^{CHP,in}$: absorbed inductive reactive power;
- $y_{b,t}^{CHP,out}$: binary variable equal to 1 when the plant provides inductive reactive power to the MG;
- $y_{b,t}^{CHP,in}$: binary variable equal to 1 when the plant absorbs inductive reactive power from the microgrid.

Constraints (14) and (15) set limits for reactive power while constraints (16) ensure that the plant cannot simultaneously supply and absorb inductive reactive power; in (14) and (15), a_b^{CHP} indicates the rated apparent power of the CHP unit.

$$0 \le q_{b,t}^{CHP,out} \le y_{b,t}^{CHP,out} \cdot \sqrt{\left(a_b^{CHP}\right)^2 - \left(p_{b,t}^{CHP}\right)^2} \quad \forall t = 1 \dots T, \forall b = 1 \dots B \tag{14}$$

$$0 \le q_{b,t}^{CHP,in} \le y_{b,t}^{CHP,in} \cdot \sqrt{\left(a_b^{CHP}\right)^2 - \left(p_{b,t}^{CHP}\right)^2} \quad \forall t = 1 \dots T, \forall b = 1 \dots B \tag{15}$$

$$y_{b,t}^{CHP,out} + y_{b,t}^{CHP,in} \le 1 \quad \forall t = 1 \dots T, \forall b = 1 \dots B \tag{16}$$

2.4. Storage model

The performance of the electrical storage system at bus b is characterized by both the maximum discharging power ($p_b^{st,dch,\max}$) and the maximum charging power ($p_b^{st,ch,\max}$), the maximum inductive reactive power that can be exchanged by the inverter ($q_b^{st,out,\max}$ when injected and $q_b^{st,in,\max}$ when absorbed) as well as by the rated capacity (C_b^{st}) and the minimum and maximum values of state of charge, respectively indicated by $soc_b^{st,\min}$ and $soc_b^{st,\max}$; a_b^{st} represents the nominal apparent power of the inverter associated with the storage system. The decision variables which are used to model the storage operation at time t are:

- $p_{b,t}^{st,dch}$: discharged active power;
- $p_{b,t}^{st,ch}$: charged active power;
- $w_{b,t}^{st,dch}$: binary variable equal to 1 when the storage is discharging;
- $w_{b,t}^{st,ch}$: binary variable equal to 1 when the storage is charging;
- $q_{b,t}^{st,out}$: supplied inductive reactive power;
- $q_{b,t}^{st,in}$: absorbed inductive reactive power;
- $y_{b,t}^{st,out}$: binary variable equal to 1 when the storage provides inductive reactive power to the MG;
- $y_{b,t}^{st,in}$: binary variable equal to 1 when the storage absorbs inductive reactive power from the MG;
- $E_{b,t}^{st}$: energy content of the battery [kWh].

Constraints (17) and (18) define the feasible values for active power while constraints (19) ensure that the charging and discharging phases cannot be simultaneous. Similar constraints are proposed for reactive power by (20)–(22). These operative constraints follow the prescriptions of CEI-021 Italian technical standard for inverter connected to the low voltage network [37].

$$0 \le p_{b,t}^{st,dch} \le p_b^{st,dch,\max} \cdot w_{b,t}^{st,dch} \quad \forall t = 1 \dots T, \forall b = 1 \dots B \tag{17}$$

$$0 \le p_{b,t}^{st,ch} \le p_b^{st,ch,\max} \cdot w_{b,t}^{st,ch} \quad \forall t = 1 \dots T, \forall b = 1 \dots B \tag{18}$$

$$w_{b,t}^{st,dch} + w_{b,t}^{st,ch} \le 1 \quad \forall t = 1 \dots T, \forall b = 1 \dots B \tag{19}$$

$$0 \le q_{b,t}^{st,out} \le q_b^{st,out,\max} \cdot y_{b,t}^{st,out} \quad \forall t = 1 \dots T, \ \forall b = 1 \dots B \tag{20}$$

$$0 \le q_{b,t}^{st,in} \le q_b^{st,in,\max} \cdot y_{b,t}^{st,in} \quad \forall t = 1 \dots T, \forall b = 1 \dots B \tag{21}$$

$$y_{b,t}^{st,in} + y_{b,t}^{st,out} \le 1 \quad \forall t = 1 \dots T, \forall b = 1 \dots B \tag{22}$$

The energy balance for the storage is reported in (23) while constraint (24) defines allowable values for state of charge. In (23), $\eta^{st,ch}$ and $\eta^{st,dch}$ respectively indicate the charging and discharging efficiency, both assumed constant.

$$E_{b,t+1}^{st} = E_{b,t}^{st} + S_{base} \cdot \Delta \cdot \left(p_{b,t}^{st,ch} \cdot \eta^{st,ch} - \frac{p_{b,t}^{st,dch}}{\eta^{st,dch}}\right) \quad \forall t = 1 \dots T-1, \forall b = 1 \dots B \tag{23}$$

$$soc_b^{st,\min} \cdot C_b^{st} \le E_{b,t}^{st} \le soc_b^{st,\max} \cdot C_b^{st} \quad \forall t = 1 \dots T, \forall b = 1 \dots B \tag{24}$$

In order avoid disruptive behaviours of the storage system, with continuous alternation of charging and discharging phases that could possibly lead to a reduction of the battery lifetime, the number of charging and discharging cycles is limited during the day. The decision variables that describe the passage to charging/discharging mode are:

- $W_{b,t}^{st,ch}$: binary variable equal to 1 if at time t there is a change of the operative state $w_{b,t}^{st,ch}$ of the BESS at node b, linked to the start or end of a charging phase, if compared to the previous time interval t-1;
- $W_{b,t}^{st,dch}$: binary variable equal to 1 if at time t there is a change of the operative state $w_{b,t}^{st,dch}$ of the BESS at node b, linked to the start or end of a discharging phase, if compared to the previous time interval t-1.

A maximum number of charging cycles $N^{max,ch}$ and a maximum number of discharging cycles $N^{max,dch}$ are provided as data.

Constraints (25) and (26) state that, if at time t-1 the BESS was either in idle mode or in discharging mode and at time t a charging cycle starts, the value of $W^{st,ch}_{b,t}$ is increased to 1. If at the following time instant $t+1$ the BESS continues to be in charge, then $W^{st,ch}_{b,t+1}$ is equal to 0. If the charging cycle ends at the time interval t^* (with $t^* > t+1$), then $W^{st,ch}_{b,t^*}$ is again equal to 1. The same procedure for the discharging phase is described by constraints (29) and (30).

The limitation on the number of charging and discharging cycles is posed by (28) and (32). The multiplication by 2 is needed since for each charging cycle, $W^{st,ch}_{b,t}$ takes value equal to 1 twice, one time at the beginning and one time at the end of the charge: the same for the discharging phase.

Constraints (27) and (31) are used only to initialize the value of $W^{st,ch}_{b,t}$ and $W^{st,dch}_{b,t}$ at $t=1$.

$$W^{st,ch}_{b,t} \geq w^{st,ch}_{b,t} - w^{st,ch}_{b,t-1} \quad \forall t = 2\ldots T, \forall b = 1\ldots B \tag{25}$$

$$W^{st,ch}_{b,t} \geq w^{st,ch}_{b,t-1} - w^{st,ch}_{b,t} \quad \forall t = 2\ldots T, \forall b = 1\ldots B \tag{26}$$

$$W^{st,ch}_{b,1} = W^{st,ch}_{b,2} \quad \forall b = 1\ldots B \tag{27}$$

$$\sum_{t=1}^{T}\sum_{b=1}^{B} W^{st,ch}_{b,t} \leq 2\cdot N^{max,ch} \tag{28}$$

$$W^{st,dch}_{b,t} \geq w^{st,dch}_{b,t} - w^{st,dch}_{b,t-1} \quad \forall t = 2\ldots T, \forall b = 1\ldots B \tag{29}$$

$$W^{st,dch}_{b,t} \geq w^{st,dch}_{b,t-1} - w^{st,dch}_{b,t} \quad \forall t = 2\ldots T, \forall b = 1\ldots B \tag{30}$$

$$W^{st,dch}_{b,1} = W^{st,dch}_{b,2} \quad \forall b = 1\ldots B \tag{31}$$

$$\sum_{t=1}^{T}\sum_{b=1}^{B} W^{st,dch}_{b,t} \leq 2\cdot N^{max,dch} \tag{32}$$

Ramp-up and ramp-down limits for charging and discharging active power are also considered, as reported in (33) and (34), where $\varsigma^{st,ch}_{b}$ and $\varsigma^{st,dch}_{b}$ are constant coefficients representing the ramp-up and ramp-down rates in charging and discharging modes.

$$p^{st,ch}_{b,t+1} - p^{st,ch}_{b,t} \leq \varsigma^{st,ch}_{b}\cdot p^{st,ch,\max}_{b} \quad \forall t = 1\ldots T-1, \forall b = 1\ldots B \tag{33}$$

$$p^{st,dch}_{b,t+1} - p^{st,dch}_{b,t} \leq \varsigma^{st,dch}_{b}\cdot p^{st,dch,\max}_{b} \quad \forall t = 1\ldots T-1, \forall b = 1\ldots B \tag{34}$$

In the MINLP model, constraints from (17) to (34) continue to apply but also constraints (35) need to be considered to model the circular capability curve of the inverter coupled with the storage system that is simply assumed to be squared in the MILP model.

$$\left(p^{st,dch}_{b,t} + p^{st,ch}_{b,t}\right)^2 + \left(q^{st,out}_{b,t} + q^{st,in}_{b,t}\right)^2 \leq \left(a^{st}_{b}\right)^2 \quad \forall t = 1\ldots T, \forall b = 1\ldots B \tag{35}$$

2.5. Load flow equations

Full LF equations implemented within the MINLP model are reported by (38) and (39) whereas linearized LF equations used by the MILP model are shown in (40) and (41). $p_{b,k,t}$ is the decision variable used for active power flowing from bus b to bus k at time t, while $q_{b,k,t}$ is the decision variable representing reactive power flowing from bus b to bus k at time t. Other decision variables are the voltage module $v_{b,t}$ and the voltage phase $\delta_{b,t}$. Parameters are given by the resistance ($r_{b,k}$) and the reactance ($x_{b,k}$) of the link connecting bus b to bus k. In detail, these two parameters are obtained starting from the per unit-length resistance r^{cable} [Ω/km] and reactance x^{cable} [Ω/km] of the cable, multiplied by $l_{b,k}$ [km], that is the length of the link between nodes b and k, and by a multiplicative coefficient w used to parametrically vary the length of the lines.

$$r_{b,k} = w\cdot l_{b,k}\cdot r^{cable} \quad \forall b,k = 1\ldots B \tag{36}$$

$$x_{b,k} = w\cdot l_{b,k}\cdot x^{cable} \quad \forall b,k = 1\ldots B \tag{37}$$

$$p_{b,k,t} = \frac{r_{b,k}}{r^2_{b,k}+x^2_{b,k}}\cdot v^2_{b,t} - v_{b,t}\cdot v_{k,t}\cdot\frac{r_{b,k}\cdot\cos(\delta_{b,t}-\delta_{k,t}) - x_{b,k}\cdot\sin(\delta_{b,t}-\delta_{k,t})}{r^2_{b,k}+x^2_{b,k}} \quad \forall t = 1\ldots T, \forall b,k = 1\ldots B \tag{38}$$

$$q_{b,k,t} = \frac{x_{b,k}}{r^2_{b,k}+x^2_{b,k}}\cdot v^2_{b,t} - v_{b,t}\cdot v_{k,t}\cdot\frac{r_{b,k}\cdot\sin(\delta_{b,t}-\delta_{k,t}) + x_{b,k}\cdot\cos(\delta_{b,t}-\delta_{k,t})}{r^2_{b,k}+x^2_{b,k}} \quad \forall t = 1\ldots T, \forall b,k = 1\ldots B \tag{39}$$

$$p_{b,k,t} = \frac{r_{b,k}}{r^2_{b,k}+x^2_{b,k}}\cdot(v_{b,t}-v_{k,t}) + \frac{x_{b,k}}{r^2_{b,k}+x^2_{b,k}}\cdot(\delta_{b,t}-\delta_{k,t}) \quad \forall t = 1\ldots T, \forall b,k = 1\ldots B \tag{40}$$

$$q_{b,k,t} = \frac{x_{b,k}}{r^2_{b,k}+x^2_{b,k}}\cdot(v_{b,t}-v_{k,t}) - \frac{r_{b,k}}{r^2_{b,k}+x^2_{b,k}}\cdot(\delta_{b,t}-\delta_{k,t}) \quad \forall t = 1\ldots T, \forall b,k = 1\ldots B \tag{41}$$

Constraint (42) defines feasible operating range for bus voltages, in order to avoid strong overvoltage and undervoltage conditions that could affect the stability of the network.

$$v^{min}_{b} \leq v_{b,t} \leq v^{max}_{b} \forall t = 1\ldots T, \quad \forall b = 1\ldots B \tag{42}$$

2.6. Power balances

Constraint (43) represents the power balance equation for each bus of the microgrid except of bus 1, that is the point of common coupling with the distribution network, whose power balance is shown in (44). In (43), $p^{L}_{b,t}$ is the active power absorbed at time t by the load connected to bus b. Reactive power balance equations are reported in (45) and (46); $q^{L}_{b,t}$ represents the inductive reactive power absorbed by the load.

$$p^{RES}_{b,t} + p^{CHP}_{b,t} + p^{st,dch}_{b,t} - p^{st,ch}_{b,t} - p^{L}_{b,t} - \sum_{\substack{k=1\\k\neq b}}^{K} p_{b,k,t} = 0 \quad \forall t = 1\ldots T, \forall b = 2\ldots B \tag{43}$$

$$p^{buy}_{t} - p^{sell}_{t} - p_{1,2,t} = 0 \quad \forall t = 1\ldots T \tag{44}$$

$$q_t^{RES,out} - q_t^{RES,in} + q_{b,t}^{st,out} - q_{b,t}^{st,in} + q_{b,t}^{CHP,out} - q_{b,t}^{CHP,in} - q_{b,t}^{L} - \sum_{\substack{k=1 \\ k \neq b}}^{K} q_{b,k,t} = 0 \quad \forall t = 1 \dots T, \forall b = 2 \dots B \tag{45}$$

$$q_t^{buy} - q_t^{sell} - q_{1,2,t} = 0 \quad \forall t = 1 \dots T \tag{46}$$

2.7. Objective function

The objective function to be minimized is given by the sum of the following main terms:

- electricity net costs, calculated as the difference between the electricity purchase costs and the revenues related to the sale of electricity to the distribution network;
- costs associated with the penalties for reactive power absorbed from the distribution network;
- curtailment costs of renewable power plants.

The main input parameters adopted to calculate these costs are:

- σ_t^{buy}: electricity purchase price [€/kWh];
- σ_t^{sell}: electricity selling price [€/kWh];
- ρ_t^{buy}: penalty for reactive power absorption [€/kVARh];
- $\tau_b^{RES,curt}$: curtailment cost of renewable power plants [€/kWh].

In (47) the objective function of the MILP model is reported split into the aforesaid components. It is possible to note that the objective function also includes other two terms: the first one related to the reactive power supplied and absorbed by generation units and storage systems, introduced to model a precedence criterion for reactive power exchange, and the second one taking into account the deviation of voltage values from 1. The first term considers a weight factor (μ_b^{RES}, μ_b^{st}, μ_b^{CHP}) for each technology while the second term includes the decision variable $u_{b,t}$, constrained by (48) and (49) and introduced to linearize $|v_{b,t}-1|$; γ is a weight factor chosen to a greater or lesser extent depending on the importance to be attached to the deviation of the bus voltage from the unit value. In the MINLP model constraints (48) and (49) are not present and the last term of the objective function is written as $\gamma \cdot \sum_{t=1}^{T} \sum_{b=1}^{B} |v_{b,t} - 1|$.

$$obj = \Delta \cdot S_{base} \cdot \sum_{t=1}^{T} \left[\left(\sigma_t^{buy} \cdot p_t^{buy} - \sigma_t^{sell} \cdot p_t^{sell} \right) + \left(\rho_t^{buy} \cdot q_t^{buy} \right) + \left(\sum_{b=1}^{B} \tau_b^{RES,curt} \cdot p_{b,t}^{RES,curt} \right) \right] + \Delta \cdot S_{base} \cdot \sum_{t=1}^{T} \times \sum_{b=1}^{B} \left[\mu_b^{RES} \left(q_{b,t}^{RES,in} + q_{b,t}^{RES,out} \right) + \mu_b^{st} \left(q_{b,t}^{st,in} + q_{b,t}^{st,out} \right) + \mu_b^{CHP} \left(q_{b,t}^{CHP,in} + q_{b,t}^{CHP,out} \right) \right] + \gamma \sum_{t=1}^{T} \sum_{b=1}^{B} u_{b,t} \tag{47}$$

$$u_{b,t} \geq v_{b,t} - 1 \quad \forall t = 1 \dots T, \forall b = 2 \dots B \tag{48}$$

$$u_{b,t} \geq -v_{b,t} + 1 \quad \forall t = 1 \dots T, \forall b = 2 \dots B \tag{49}$$

3. Results and Discussion

This section presents the results of the study. It is divided into four subsections: the first two subsections present respectively the numerical values that have been chosen for the input quantities and the numerical results for the simplified network with 4 nodes, comparing the non-linearized and the linearized results in order to find which is the best approach. The third and the fourth subsections present the input data and the numerical results for the complete network, modelled with linearized equations.

Before presenting the input data and the results, a flowchart of the method is provided (see Fig. 2), in order to enhance the reader's comprehension. Starting from the input quantities, which include technical data about generation technologies and MG infrastructures, economic data about the exchange of active and reactive energy with the external network and load data regarding the active and reactive power demands, the EMS ensures the optimal operation of the MG, defining the optimal profiles of generation of PV and WT units, the optimal charging/discharging profile of the BESS and the optimal active and reactive power flows between the nodes and between the MG and the external network.

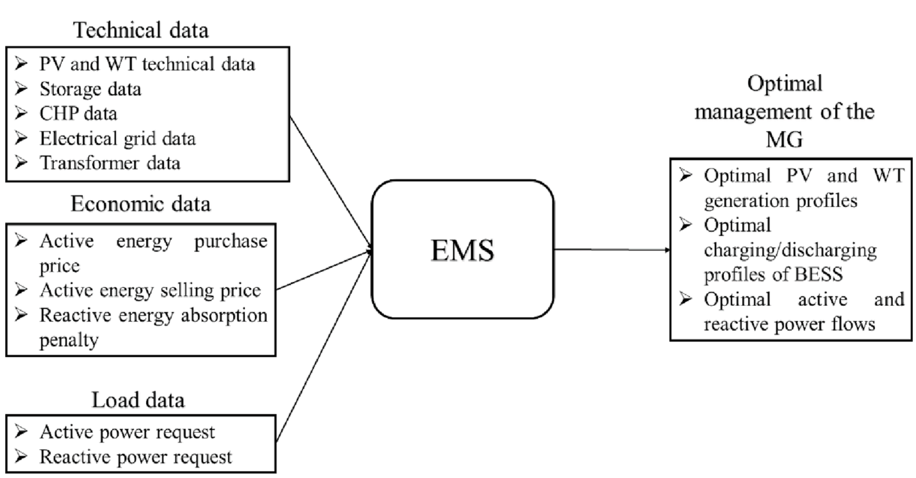

Fig. 2. Flowchart of the method.

3.1. Input data – Simplified network

Before showing the results for the simplified network, it is necessary to describe some numerical input data to facilitate the reader's understanding.

The considered simplified facility includes a PV plant, a load and a step-down transformer, connected on the primary side to the medium voltage grid. The topology of the network is represented in Fig. 3.

The PV source features an inverter with a power rating of 200 [kVA]. The profile of the PV available active power generation has been estimated using the PVGIS Online Tool database [38].

The load has been characterized as a resistive-inductive load, with a peak absorbed active power equal to 200 [kW], working at nominal power factor equal to 0.9 and with a daily active energy absorption equal to 2574.1 [kWh].

The transformer's rating is equal to 250 [kVA], with a transformation ratio of 15/0.4 kV/kV. The transformer is modelled as ideal.

The length of Line 1–2 is 70 [m]; the length of Line 2–3 is 200 [m]; the length of Line 1–3 is 150 [m]. Cables have been modelled with unitary (per unit length) resistance and reactance respectively equal to 0.096 [Ω/km] and 0.069 [Ω/km].

Voltage limits have been set as follows: $v_{b,min}$=0.9 [p.u.] and $v_{b,max}$ = 1.1 [p.u.].

The unitary price for the purchase of active energy from the network σ_t^{buy} has been put equal to 0.225 [€/kWh], constant for the whole day. The unitary cost of purchase of reactive energy from the network ρ_t^{buy} has been considered equal to 0.049 [€/kVARh] during intermediate hours and peak hours and equal to 0 during off-peak hours (i.e. during the night). The unitary revenue deriving from the sale of electricity to the network σ_t^{sell} has been considered equal to 0.05 [€/kWh] and constant for the whole day. The curtailment cost for the PV source $\tau_b^{RES,curt}$ has been considered equal to the Levelized Cost of Electricity (LCOE) for the PV source, namely 0.128 [€/kWh] [39].

The optimization has been performed over a single day, with a time resolution of 10 minutes $\left(\Delta = \frac{1}{6}\ [\mathrm{h}]\right)$.

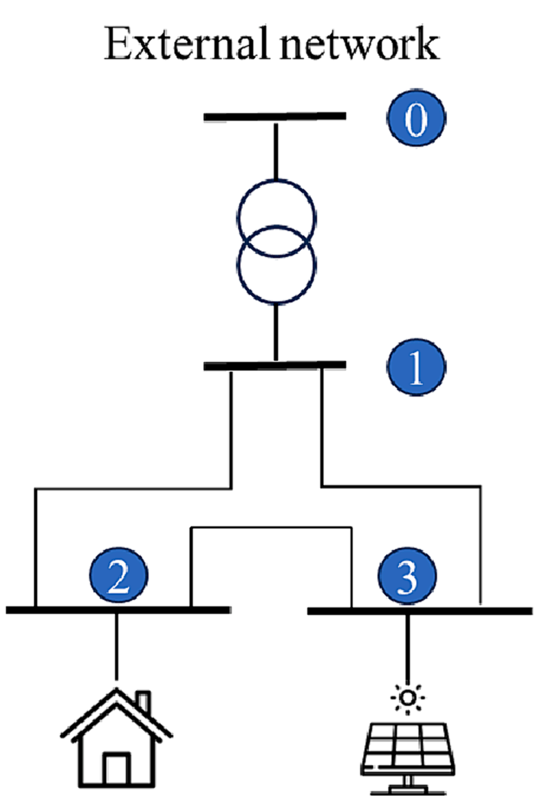

Fig. 3. Simplified network topology.

Both the linear and non-linear models have been implemented in Matlab R2022b/Yalmip (R20210331 release) environment [40]. The linear optimization problem has been modelled as a MILP problem and has been solved calling the Gurobi solver [41], whilst the MILNP problem has been solved calling the BONMIN solver [42]. Yalmip is a toolbox that can be added to Matlab, for the formalization and implementation of optimization problems. Gurobi solver is able to solve Linear Programming (LP) problems, MILP problems and more complex problems up to Mixed-Integer Quadratically Constrained Programming (MIQCP) problems. BONMIN is an open-source solver for the resolution of MILNP problems.

Some computational parameters are resumed in Table 1, considering three possible lengths of the lines, varying the coefficient *w*.

As it is evident from the values reported in Table 1, the computational times required for the solution of the linear model by Gurobi are basically negligible. On the other hand, BONMIN requires a long time to solve the non-linear problem, with an increasing computational effort in the scenarios in which lines are longer.

The number of variables takes into account both continuous and binary variables. The number of constraints is made of the sum of the number of inequality and equality constraints.

3.2. Results – Simplified network

This subsection provides some numerical and graphical results for the simplified network, discussing how the results change depending on the chosen model (linear/nonlinear) and how they change with an increasing length of the lines.

Considering the base length of the lines (i.e. $w = 1$), in Fig. 4 the daily trends of the voltage amplitudes are reported. Voltage amplitudes are all within the limits, being very close to 1 [p.u.]: in detail, the voltage amplitude at node 1 is constant at 1 [p.u.] because that node has been considered as the slack node; at node 2, undervoltage conditions are evident for the whole day, due to the presence of the load; at node 3 overvoltage can be highlighted during the central hours of the day, due to the presence of PV generation, while during night undervoltage conditions are evident because in those hours the PV is not allowed to inject inductive reactive power to support the voltage.

Fig. 5 shows the daily trend of the voltage phases at the three nodes. At node 1 the phase is blocked at 0 [deg], being node 1 the slack node. At the other two nodes, the phase variation is limited to some decimals of degree.

In Fig. 6 and Fig. 7 the profiles of the active and reactive power flows over the three lines are presented. It is important to highlight that according to the linear model there is no difference between active and reactive power flows evaluated at the sending and receiving nodes (e.g. $|P_{ij}|=|P_{ji}|$). Looking at the results of the nonlinear model, it can be noted that at the sending node *i*, the active and reactive power flows that leave the node towards the receiving one are larger (in absolute value) than the ones obtained with the linear model, because full LF equations are considered. In any case, the deviation between linear and nonlinear results is minor.

Finally, Fig. 8 reports the results of the EMS, showing a comparison

Table 1
Computation parameters.

	Linear model	Non-linear model
Number of variables	6480	5230
Number of constraints	4752	5406
Computation time ($w = 1$)	0.59 s	350 s
Computation time ($w = 2$)	0.57 s	397 s
Computation time ($w = 3$)	0.58 s	446 s
Computation time ($w = 10$)	0.60 s	681 s

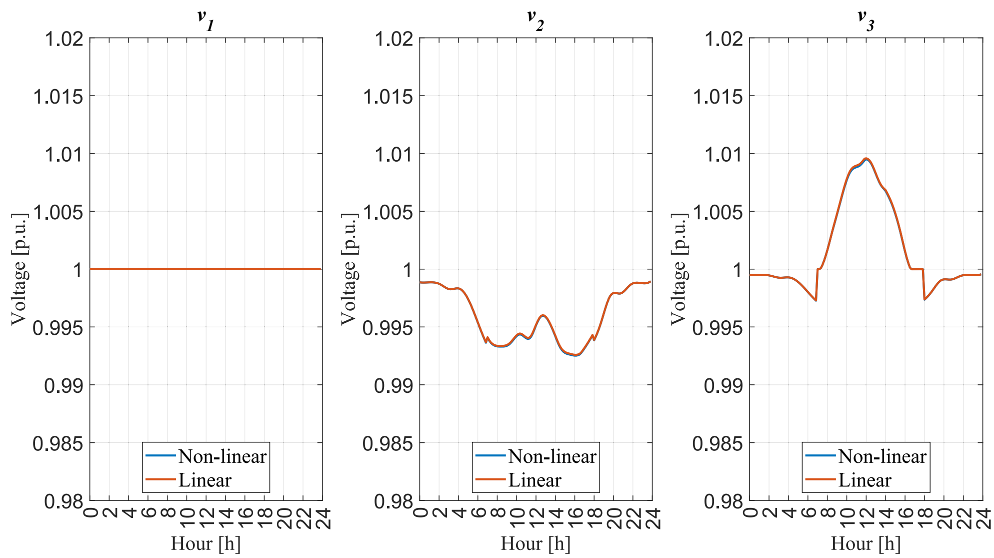

Fig. 4. Voltage amplitudes trends at nodes 1, 2 and 3.

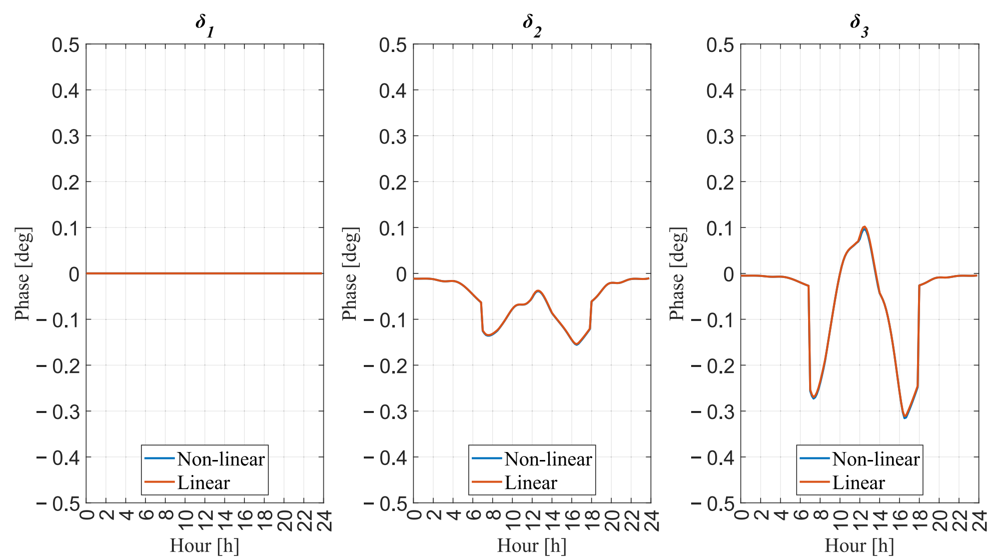

Fig. 5. Voltage phases trends at nodes 1, 2 and 3.

between the two models. Focusing on the active power, the trend of PV production is the same, because the PV source is exploited as much as possible, with no curtailment. It is interesting to highlight that, according to the linear model, between 12 PM and 1 PM a small amount of energy is sold to the external network; this possibility is not highlighted in the non-linear model results because the implemented formulation takes into account the full LF equations, meaning that there is always the need of purchasing energy from the network.

Looking at the reactive power trends, it can be highlighted that during the day in both EMS formulations the reactive power injection by the PV is limited at the maximum value, except of the central hour around 1 PM in which the request of reactive power from the load is reduced and therefore also PV reactive power injection is reduced. Similarly to the active power trend, the reactive power that has to be injected by the PV inverter and the reactive energy that has to be purchased from the external network are larger in the non-linear model rather than in the linear one, due to the deviation introduced by full LF equations.

Table 2 presents the daily values of the main energy quantities for different scenarios in which the length of the lines has been increased, doubling and tripling the w coefficient.

Table 3 highlights the percentage difference between the results of the linear and of the non-linear models. All the percentages deviations are calculated as in (50), where μ is a generic quantity and the subscripts NL and L stay for "non-linear" and "linear".

$$\mu_{\%} = 100 \cdot \frac{\mu_{NL} - \mu_{L}}{\mu_{NL}} \tag{50}$$

Table 2 lists the main energy results of the EMS, applied to the simple MG. Active and reactive energy requests of the load are input data. The PV never undergoes curtailment, in any considered scenario, meaning that the PV works always at the maximum power point. Quantities that depend on losses vary depending on the considered model (linear or nonlinear) and depending on the length of the lines. The amount of active and reactive energy withdrawn from the network and the amount of reactive energy injected by the PV unit reach the lowest values when considering the linear results, since losses are not considered. Similarly, the amount of active energy sold to the external network is maximum when considering a linear model. NCs are the lowest ones in the linearized scenario. Besides, since in the linear model the active and reactive

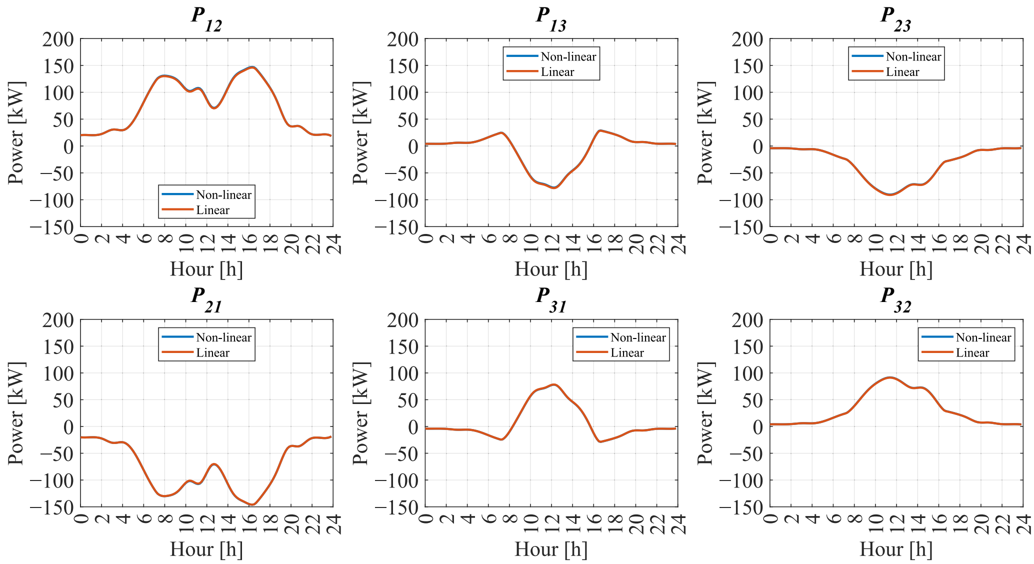

Fig. 6. Active power flows on the three lines.

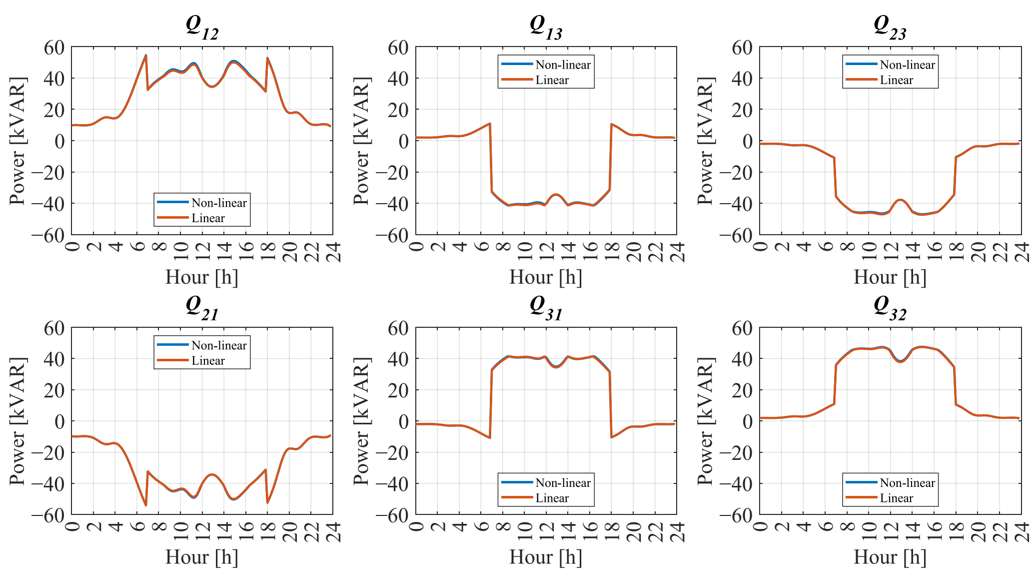

Fig. 7. Reactive power flows on the three lines.

power flows at the sending nodes and receiving nodes of a connection are equal in absolute value, the linear results do not change while increasing the lines' length. On the other hand, in the non-linear model, increasing w there is a corresponding increase in the active and reactive energies that have to be purchased from the network, in order to compensate the increased losses that are proportional to the length of the lines. In the non-linear scenario, there is also a decrease of the sold energy when the length of the lines is doubled; for further increase of the lines' length, active energy is no more sold. There is also an increase in the amount of reactive energy delivered by the PV: this energy is provided during those hours in which the PV inverter is not saturated (see Fig. 8), so around 1 PM and in the early morning and late afternoon. NCs gradually increase due to the additional energy that has to be bought from the external network in order to compensate losses.

Focusing on Table 3, it can be highlighted that the percentage deviation of the linear results if compared to the non-linear ones is reduced for $w = 1$, being limited within less than the 3% (excluding sold active energy, for which the percentage deviation is very large due to the low absolute values of the two quantities): this means that the application of a MILP problem is effective in reducing the computational effort of the calculator, while granting a satisfactory accuracy of the results, with a reduced deviation between the nonlinear and the linear results. This accuracy is slightly reduced when considering larger values of *w,* being the linear results' deviation from the non-linear ones anyway limited within the 8%. Strongly increasing the length of the lines up to 10 times the original one, the deviation becomes unacceptable, upcoming the 25% for the amount of reactive energy bought from the network.

In conclusion, the linearization of the LF equations gives acceptable results when the length of the lines is limited to 3 times the original length (<1km), which reflects the typical size of MG. When the length of the lines is increased ten-fold, the deviation between the linear and the non-linear results become unacceptable and therefore the linearization of LF equations is no more useful and effective.

Starting from these considerations, the EMS for the optimal operation of the "Full" network, whose results are presented in Section 3.3 and Section 3.4, has embedded in its mathematic formulation the linearized version of the LF equations, being the length of the lines limited and in order to reduce the computational effort.

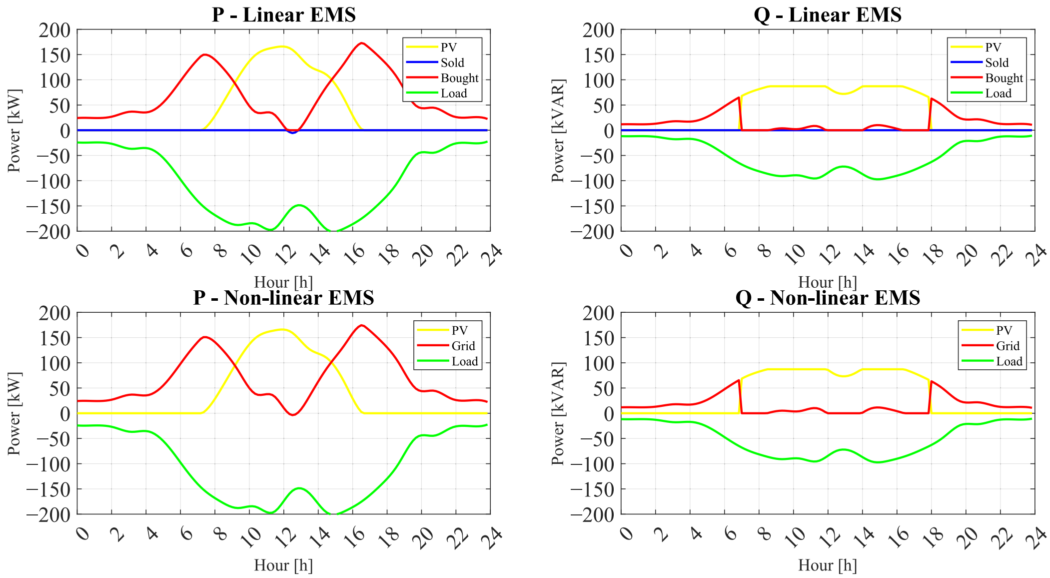

Fig. 8. Active and reactive power injections for linear and non-linear models.

Table 2
Comparison of energy quantities and NCs with linear and non-linear models, varying *w*.

Energy quantities and NCs	[–]	$w = 1$		$w = 2$		$w = 3$		$w = 10$	
		L	NL	L	NL	L	NL	L	NL
Load active energy demand	[kWh]	2574.1	2574.1	2574.1	2574.1	2574.1	2574.1	2574.1	2574.1
Load reactive energy demand	[kVARh]	1246.7	1246.7	1246.7	1246.7	1246.7	1246.7	1246.7	1246.7
PV active energy production	[kWh]	956.13	956.13	956.13	956.13	956.13	956.13	956.13	956.13
PV curtailed active energy	[kWh]	0	0	0	0	0	0	0	0
PV reactive energy production	[kVARh]	905.99	911.47	905.99	916.72	905.99	921.54	905.99	947.11
Bought active energy	[kWh]	1620.30	1639.10	1620.30	1660.22	1620.30	1681.03	1620.30	1839.22
Sold active energy	[kWh]	2.33	1.33	2.33	0.45	2.33	0	2.33	0
Bought reactive energy	[kVARh]	340.70	350.18	340.70	360.02	340.70	370.48	340.70	458.61
NCs	[EUR]	365.81	370.85	365.81	375.74	365.81	380.84	365.81	420.00

3.3. Input data – "Full" network

In this subsection, a description of the "full" MG topology is provided, along with the presentation of the major technical input data. The MG is modelled as a multi-busbar network. At each node different technologies are installed. Globally, electric loads, PV units, a WT, a BESS and a CHP unit are present in the MG. The connection of the MG to the external medium voltage network is granted by a step-down transformer. Fig. 9 graphically defines the nodes at which each technology is connected.

The PV sources installed at nodes 3, 5 and 6 feature inverters with a power rating respectively of 26 [kVA], 100 [kVA] and 14 [kVA]. The profile of the PV available active power generation has been determined by the PVGIS Online Tool database [38].

The WT installed at node 4 is equipped with an inverter whose rating is equal to 10 [kVA]. The profile of the wind speed has been estimated using the PVGIS Online Tool database. A generic power curve for a vertical-axis WT has been considered in order to find the active power production profile.

RESs are exploited not only to generate active power but also to satisfy the reactive power request of the load, thanks to the reactive power exchange capability of the inverters: in addition, by adjusting their reactive power injection/absorption, they provide voltage regulation at the node at which they are connected, even during night [43 44].

The CHP active power production profile has been obtained assuming a thermal load to be satisfied, in thermal priority mode. Therefore, the active power production is proportional to the thermal power production. Profiles derive from real data, measured at the Savona Campus facility of the University of Genoa [39]. The peak power provided by the CHP is equal to 18 [kW]. CHP inverter is able to exchange reactive power, following a semi-circular capability curve.

The BESS installed at node 5 has a capacity equal to 360 [kWh], with a maximum charging/discharging power of 50 [kW]. The inverter of the BESS is able to exchange reactive power, up to 50 [kVAR]. A squared capability curve has been considered, meaning that active and reactive power exchanges are independent on each other. $soc_b^{st,\min}$ is chosen equal to 10% and $soc_b^{st,\max}$ equal to 100%. $N^{max,ch}$ and $N^{max,dch}$ are set equal to 4 each, meaning that only two charging cycles and two discharging cycles are allowed. The coefficients $\varsigma^{st,ch}$ and $\varsigma^{st,dch}$ that limit the charge and discharge power are equal to 10%.

The loads have been characterized as resistive-inductive loads, with a peak absorbed active power equal to 63 [kW] for load installed at node 3 and 30 [kW] at node 6, working at nominal power factor equal to 0.9.

Table 3
Percentage deviation between linear and non-linear results, varying *w*.

Energy quantities and NCs	[–]	$w = 1$	$w = 2$	$w = 3$	$w = 10$
PV active energy production	[%]	0	0	0	0
PV curtailed active energy	[%]	0	0	0	0
PV reactive energy production	[%]	0.60	1.17	1.69	4.34
Bought active energy	[%]	1.21	2.41	3.61	11.9
Sold active energy	[%]	271.42	626.06	N/C[1]	N/C[1]
Bought reactive energy	[%]	2.71	5.37	8.04	25.7
NCs	[%]	1.36	2.64	3.95	12.9

[1] N/C because in the non-linear results, the sold active energy is equal to 0.

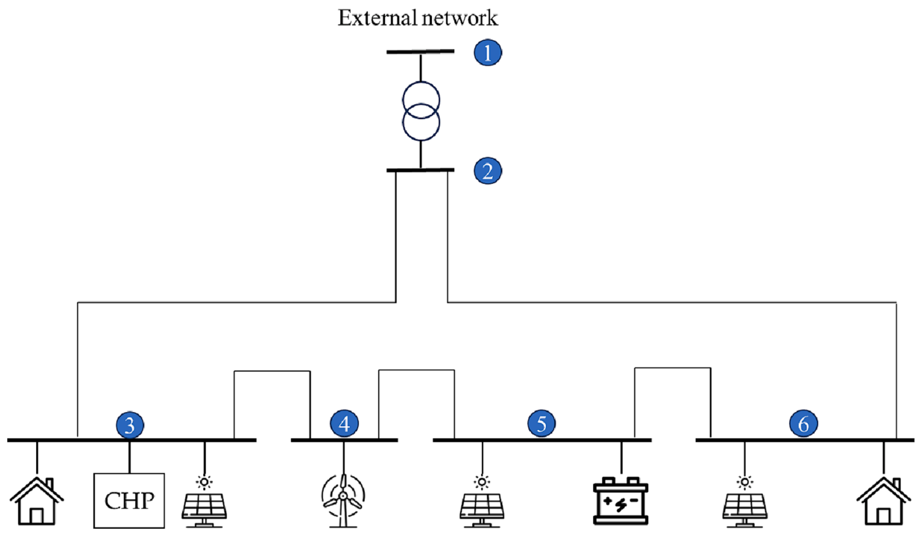

Fig. 9. "Full" network topology.

The daily active energy absorptions are equal respectively to 795 [kWh] and 418 [kWh].

The transformer's rating is equal to 250 [kVA], with a transformation ratio of 15/0.4 [kV/kV], a short-circuit voltage equal to 4% and losses equal to 3.4 [kW].

The length of Line 2–3 is 75 [m]; the length of Line 2–6 is 300 [m]; the length of Line 3–4 is 150 [m]; the length of Line 4–5 is 150 [m]; the length of Line 5–6 is 75 [m].

Cables have been modelled with unitary (per unit length) resistance and reactance respectively equal to 0.250 [Ω/km] and 0.083 [Ω/km].

Voltage limits have been set as follows: $v_{b,min}$=0.9 [p.u.] and$v_{b,max}$ = 1.1 [p.u.].

The unitary price for the purchase of active energy from the network σ_t^{buy} has been considered variable during the day: it is equal to 0.32 [€/kWh] during peak hours, 0.26 [€/kWh] during off-peak hours and 0.30 [€/kWh] during intermediate hours. The unitary price for the purchase of reactive energy from the network ρ_t^{buy} has been put equal to 0.049 [€/kVARh] during the central hours of the day and equal to 0 during off-peak hours (i.e. during night), while the unitary revenue deriving from the sale of electricity to the network σ_t^{sell} has been considered equal to 0.12 [€/kWh]. The two latter prices are considered constant for the whole day. Curtailment costs for RESs $\tau_b^{RES,curt}$ are considered equal to the LCOE of the different sources, respectively 0.6 [€/kWh] for the wind source and 0.128 [€/kWh] for the PV source [39].

In order to define a dispatching priority for reactive power provision, coefficients μ_b^{RES}, μ_b^{st} and μ_b^{CHP} have been chosen such that $\mu_b^{CHP} < \mu_b^{RES} < \mu_b^{st}$. Their value is very small, so that the impact on the objective function is low.

The optimization has been performed over a single day, with a time resolution of 10 minutes $\left(\Delta = \frac{1}{6}[\mathrm{h}]\right)$.

The MILP problem has been implemented in Matlab R2022b/Yalmip (R20210331 release) environment [40], solved calling the Gurobi solver [41]. Having a linear formulation, the computational time required for the solution of the model is basically negligible.

The number of variables is equal to 13102, taking into account both continuous and binary variables. The number of constraints is made of the sum of the number of inequality and equality constraints and is equal to 19292.

3.4. Results – "Full" network

This subsection provides some numerical and graphical results for the full network. Different objective function formulations have been considered: first, the objective function aims to minimize the operating costs of the MG ("EMS 1"); then, a term is added to try to minimize the voltage deviation from the rated value ("EMS 2"). Energy and cost quantities will be discussed in the subsubsection 3.4.5, comparing the results of different objective function formulations.

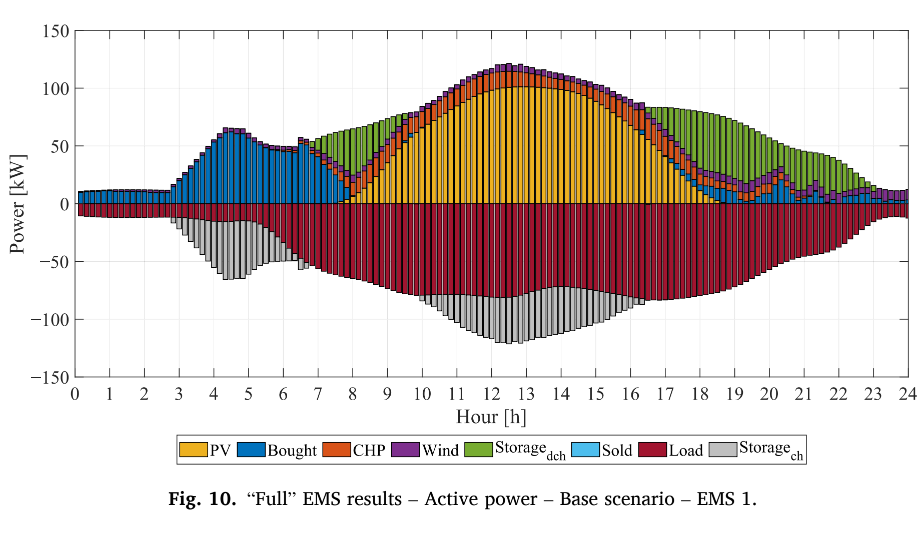

Fig. 10. "Full" EMS results – Active power – Base scenario – EMS 1.

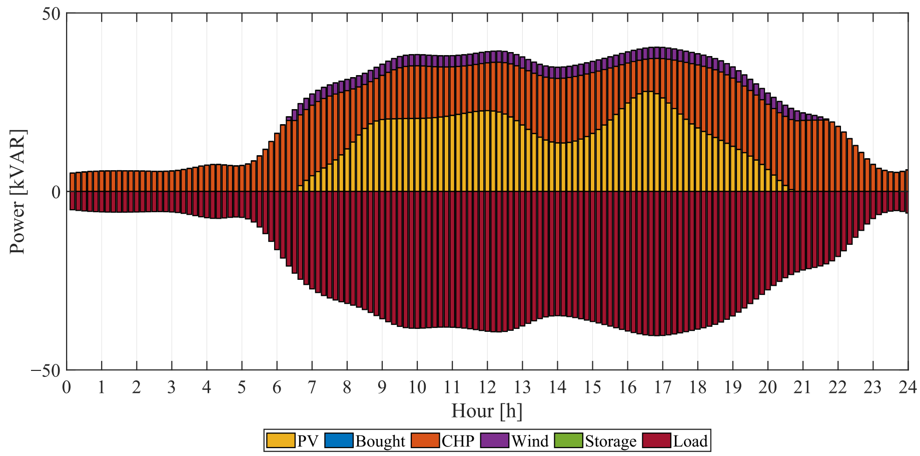

Fig. 11. "Full" EMS results – Reactive power – Base scenario – EMS 1.

3.4.1. Minimization of operating costs of the MG

This subsubsection analyses the results of the EMS taking into account in the objective function only the operating costs, related to the purchase and sale of active and reactive energy, and the curtailment costs. In this case, the weight coefficient γ has been set equal to 0.

Fig. 10 and Fig. 11 report the results of the EMS, showing the optimal active and reactive power productions of the sources installed in the MG.

The active power production of the CHP is fixed because the unit works in thermal priority mode, meaning that once the thermal dispatchment is performed, the electrical active power generation profile is determined. During the night the CHP unit is not working, therefore its active power production is 0. Wind power production profile follows the trend of the source's availability, with no curtailment. The load profile is given by the sum of the active power demand at node 3 and node 6. The PV production profile is given by the sum of the three productions of the PV units at node 3, 5 and 6. Again, curtailment is not applied. Active energy is purchased from the external network especially during the early morning and the evening, when the price of electricity is low. During the night and the early morning, that energy is used both to satisfy the electric load, along with the WT production, and to charge the BESS. BESS is charged also during the central hours of the day in order to avoid PV curtailment. BESS is discharged around from 7 AM to 10 AM, when the price of electricity starts to increase and the PV production is still low; BESS is discharged also during the late afternoon and the evening.

Considering reactive power, a priority order has been set by the authors in order to dispatch the inductive-reactive power exchange of the different sources' inverters. The first source to provide reactive power is the CHP unit, then the PV units and finally the WT, that closes the balance. In this way, reactive power is never bought from the network.

The ON/OFF status of the DER units and of the exchange with the network is reported in Fig. 12.

Fig. 13 and Fig. 14 show the trends of active and reactive power flows between nodes. Focusing on active power, the flow across the transformer is positive during the early morning, the evening and the night, due to the need of purchasing active energy. During the central part of the day, no active energy is purchased from the network and therefore the flow across the transformer is 0. The flow between node 2 and node 3 is always positive, because at node 3 a large load in installed. $P_{3,4}$ and $P_{4,5}$ are positive during the night and early morning because power is required at node 5 for the charging of the BESS. For the same reason, $P_{6,2}$ is negative in the first hours of the day. During the central hours of the day, $P_{3,4}$ and $P_{4,5}$ become negative, so the flow is directed towards node 3 to satisfy the therein-located demand: for the same reason $P_{6,2}$ becomes positive, in order to feed load 3 exploiting the ring configuration of the MG. $P_{5,6}$ is negative up to 6 AM, when the battery requires power to be charged. Then, during the central and final part of

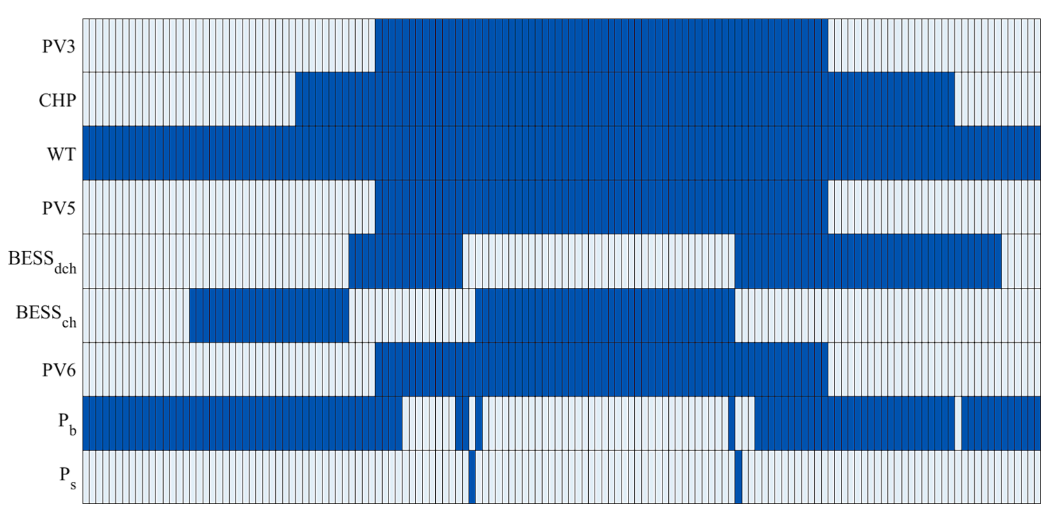

Fig. 12. "Full" EMS results – ON/OFF status of the units and of the network. Blue means that in that time interval the unit is ON or that the relevant exchange is different from 0, whilst white means that in that interval the unit is OFF or the relevant exchange is equal to 0 – Base scenario – EMS 1. (For interpretation of the references to colour in this figure legend, the reader is referred to the web version of this article.)

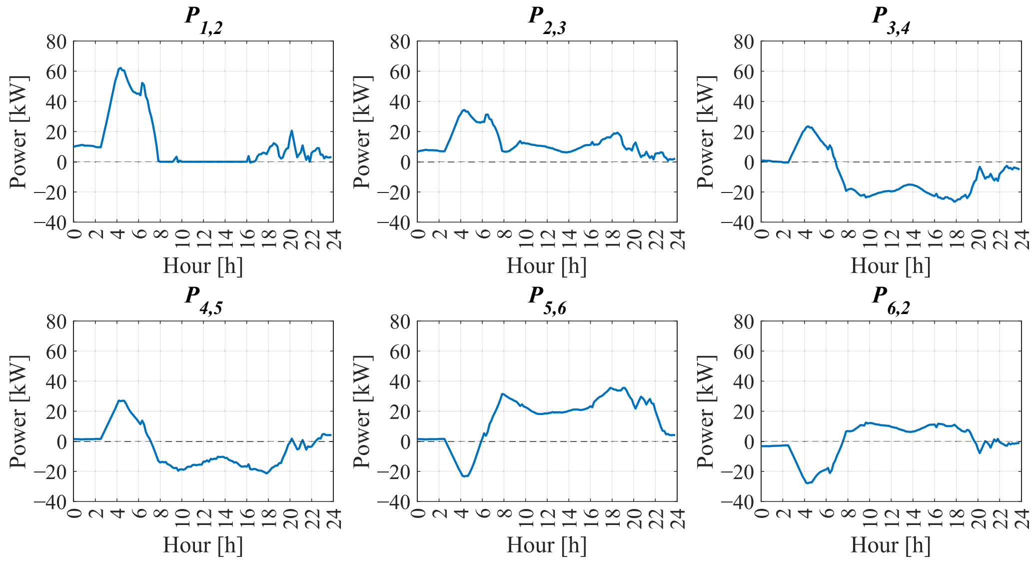

Fig. 13. "Full" EMS results – Active power flows on the lines – Base scenario – EMS 1.

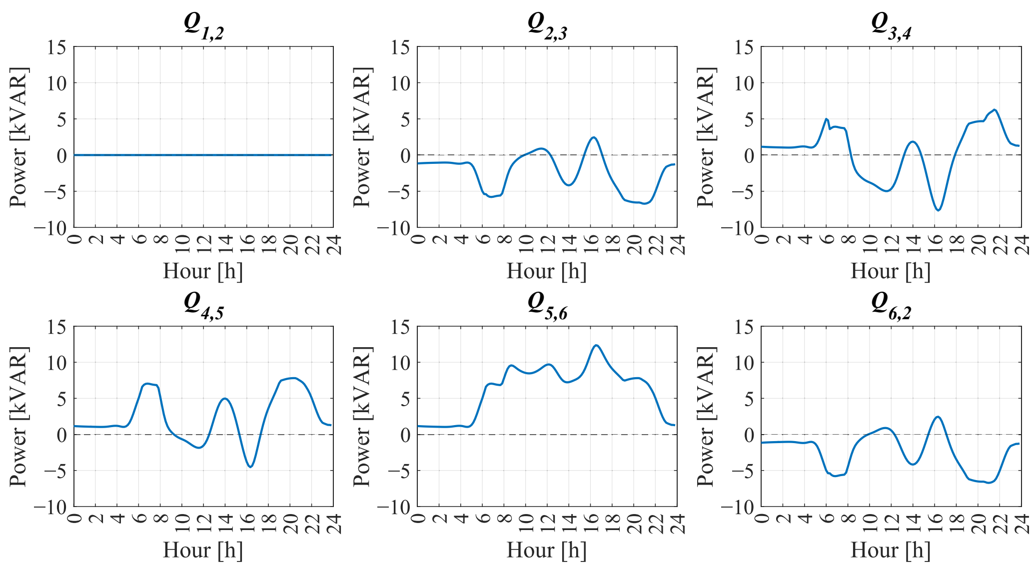

Fig. 14. "Full" EMS results – Reactive power flows on the lines – Base scenario – EMS 1.

the day, thanks to the PV production and to the BESS discharge, this power flow is always positive and directed towards node 6, satisfying the local load and partially moving towards node 2, exploiting the ring configuration of the MG.

Reactive power flows have instead a fluctuating trend, becoming either negative or positive during the day. $Q_{1,2}$ is always 0 because reactive energy is never purchased from the external network, since the satisfaction of the reactive power demand is shared among the inverters installed in the MG.

Fig. 15 and Fig. 16 report the trends of voltage modules and phases at each node.

Voltage modules lay within a range quite close to 1, far from upper and lower bounds: in particular, at node 5 the largest voltage deviation can be highlighted, both in under-voltage conditions (0.98 [p.u.]) and in over-voltage conditions, reaching 1.01 [p.u]. During the night and the early morning, voltage modules at nodes 4, 5 and 6 drop down since the storage installed at node 5 is in charging mode, behaving like a load. During the central hours of the day, on the other hand, voltage modules at these nodes go beyond 1 [p.u.]: at node 5, the BESS discharges and PV injects large amount of active power; at nodes 6, besides of the presence of a PV plant, the voltage rises due to the incoming active power flow from node 5. For the same reason, v_4 rises due to the local WT production and due to the incoming active power flow from node 5, that flows through node 4 towards node 3, where a large load is installed. v_3 is always below 1 [p.u.], due to the action of the load. v_2 is reduced if compared to v_1 due to the voltage drop across the transformer.

Voltage phases are always very close to 0, thus laying in an acceptable interval.

3.4.2. Minimization of operating costs of the MG + Minimization of voltage deviation

This subsubsection analyses the results of the EMS taking into account in the objective function both the operating costs, related to the purchase and sale of active and reactive energy and to curtailment costs, and the minimization of voltage deviation. The weight coefficient γ has been set equal to 10, such that the terms of the objective function lay in the same order of magnitude.

The results of the EMS are presented in Fig. 17 and Fig. 20, showing

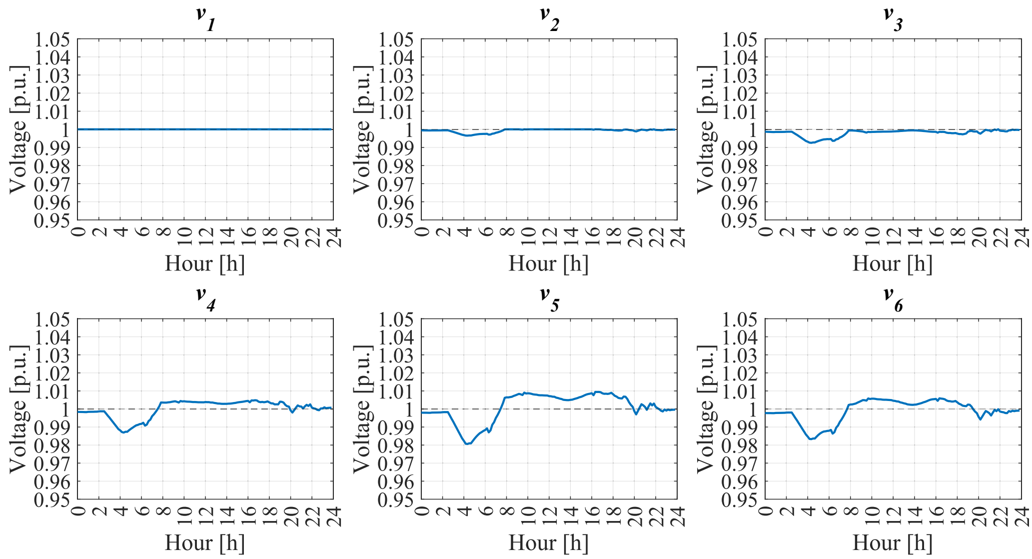

Fig. 15. "Full" EMS results – Voltage amplitudes at nodes 1, 2, 3, 4, 5 and 6 – Base scenario – EMS 1.

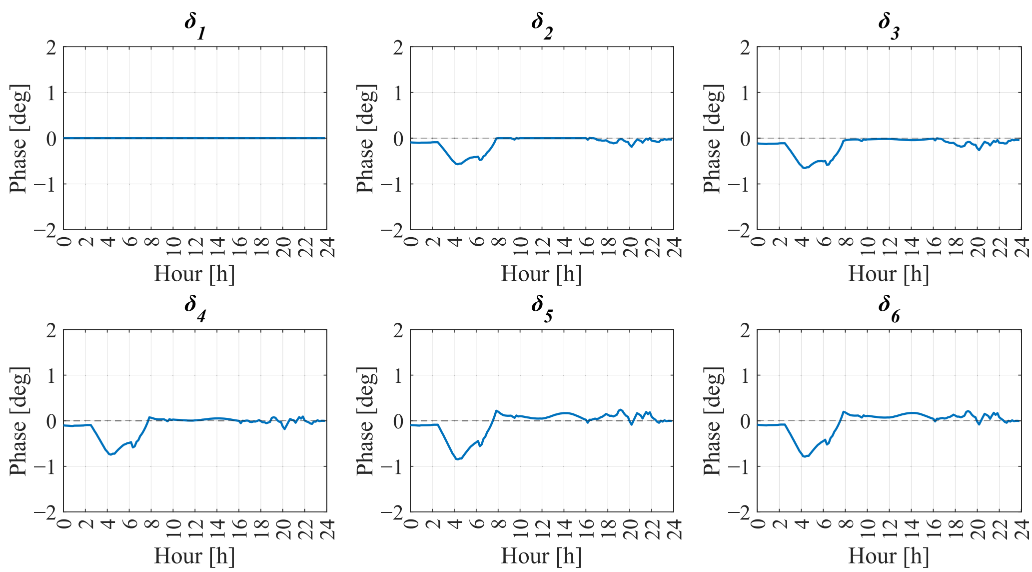

Fig. 16. "Full" EMS results – Voltage phases at nodes 1, 2, 3, 4, 5 and 6 – Base scenario – EMS 1.

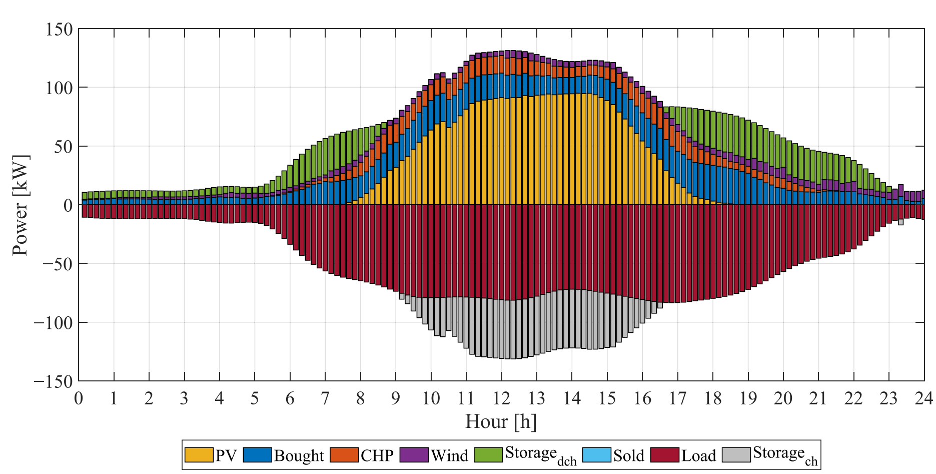

Fig. 17. "Full" EMS results – Active power – Base scenario – EMS 2.

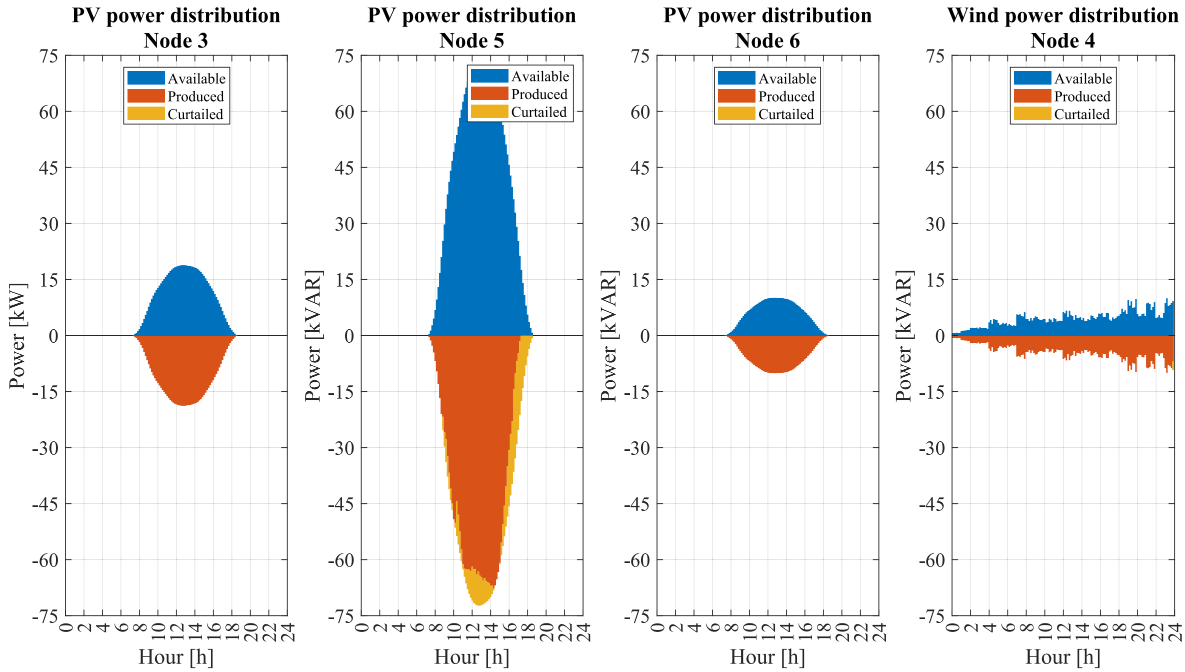

Fig. 18. "Full" EMS results – RES power distribution – Base scenario – EMS 2 – In the positive direction of the vertical axis, the available power is reported. In the negative direction, the actual production of the sources and the curtailed power are reported, for each time interval. Negative values are used only for a comparison, being physically meaningless.

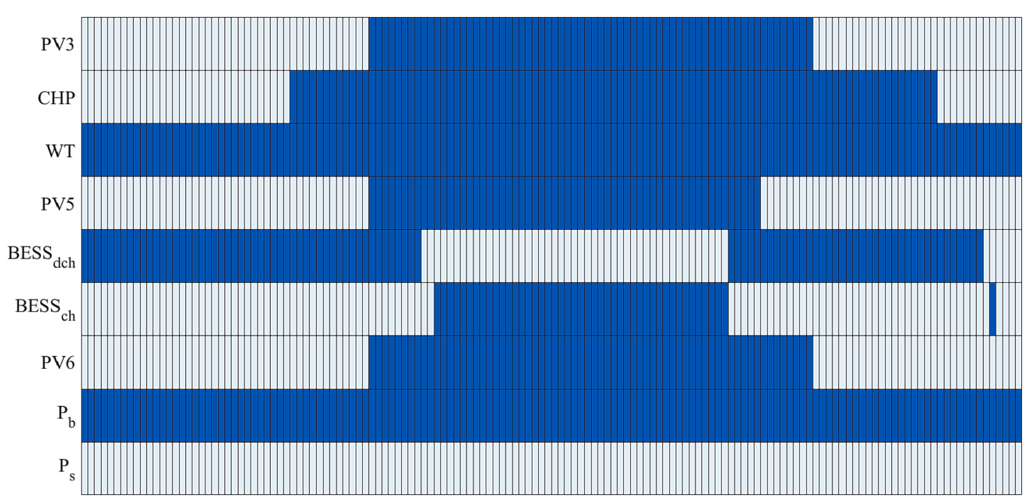

Fig. 19. "Full" EMS results – ON/OFF status of the units and of the network. Blue means that in that time interval the unit is ON or that the relevant exchange is different from 0, whilst white means that in that interval the unit is OFF or the relevant exchange is equal to 0 – Base scenario – EMS 2. (For interpretation of the references to colour in this figure legend, the reader is referred to the web version of this article.)

the optimal active and reactive power productions of the sources installed in the MG.

CHP and load active power profiles are the same as in the previous scenario. The PV production profile is given by the sum of the three productions of the PV units at node 3, 5 and 6. As it is shown in Fig. 18, the PV installed at node 5 undergoes curtailment for almost the whole day (except of the morning), in order to reduce overvoltages at node 5. The BESS is charged only during the central portion of the day and not during the night, in order to reduce the nightly voltage drop at node 5, while contributing to smooth the voltage increase, related to PV production during day-light hours. On the other hand, BESS is discharged from 12 AM to 8:30 AM and from 5 PM to 12 AM in order to reduce the purchase of active energy from the external network, while supporting the voltage at the installation node. Nevertheless, in order to reduce the voltage deviation at the busses, active energy is always purchased from the external network during the day.

The ON/OFF status of the DER units and of the exchange with the network is presented in Fig. 19.

Considering reactive power, the same priority order has been considered. It can be highlighted that the provision of reactive power by CHP and PV units is almost the same, with a small increase for the PV source. In fact, the WT inverter's contribution is reduced in time, ending earlier than in the previous case: during these hours, the WT injection reduction is compensated by an increase of the PV injection. In order to support the voltage, some reactive energy has to be purchased from the network around 5 AM and between 11 PM and 12 AM, when it is free.

Fig. 21 and Fig. 22 show the trends of active and reactive power flows between nodes. Focusing on active power, the flow across the

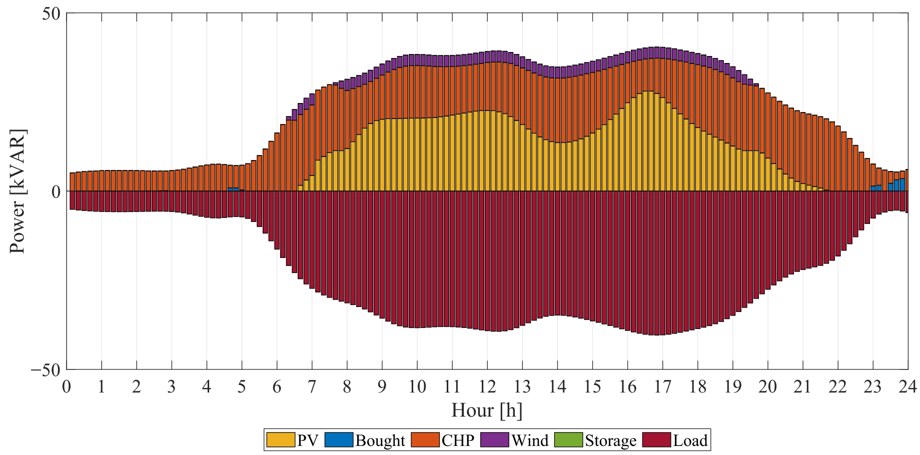

Fig. 20. "Full" EMS results – Reactive power – Base scenario – EMS 2.

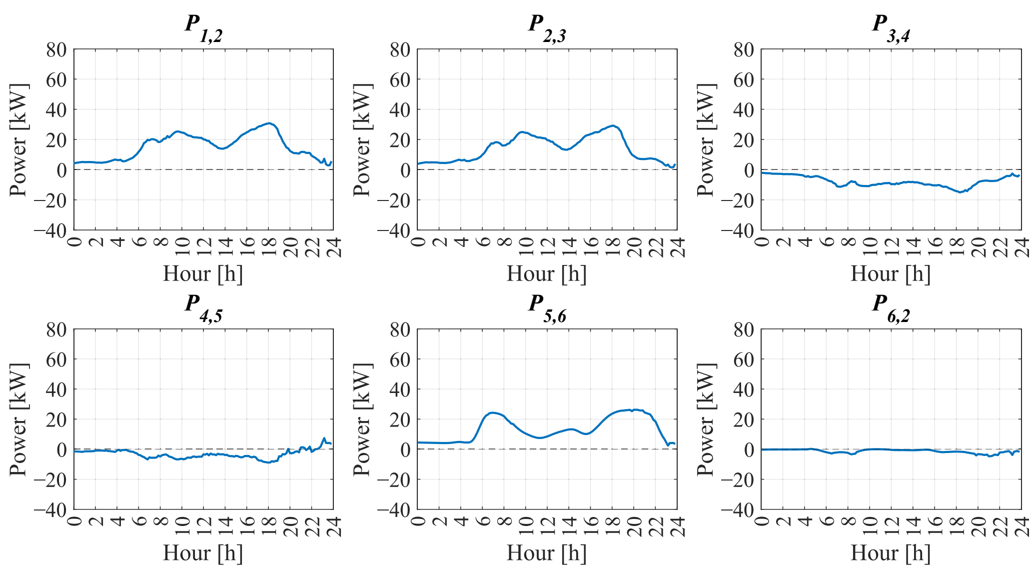

Fig. 21. "Full" EMS results – Active power flows on the lines – Base scenario – EMS 2.

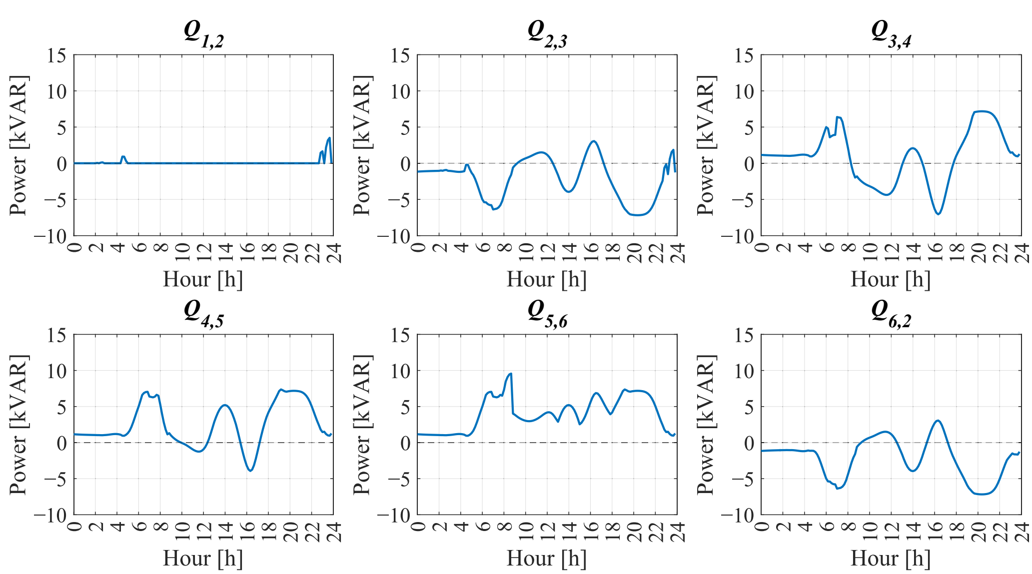

Fig. 22. "Full" EMS results – Reactive power flows on the lines – Base scenario – EMS 2.

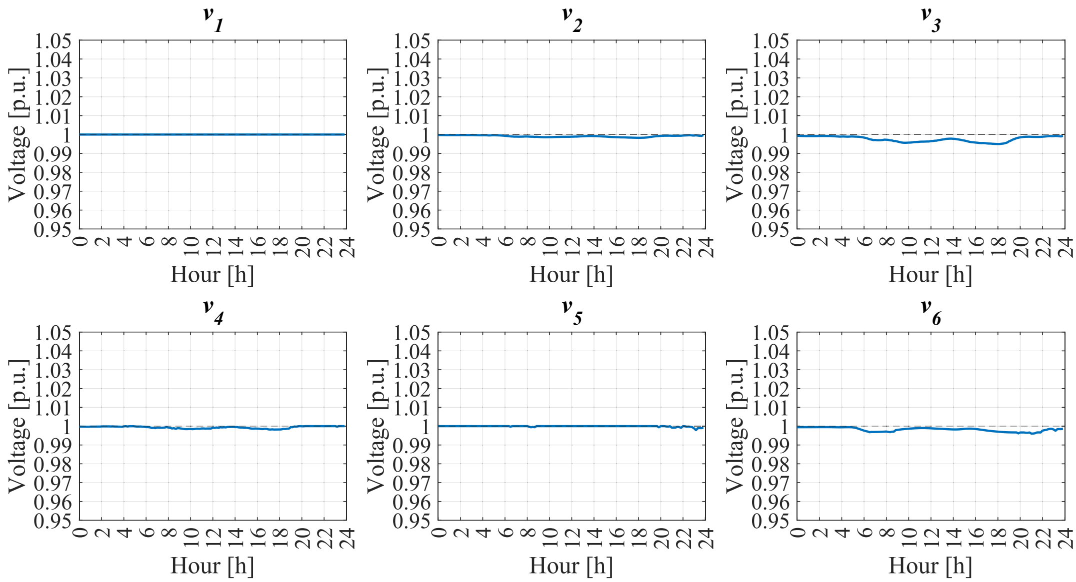

Fig. 23. "Full" EMS results – Voltage amplitudes trends at nodes 1, 2, 3, 4, 5 and 6 – Base scenario – EMS 2.

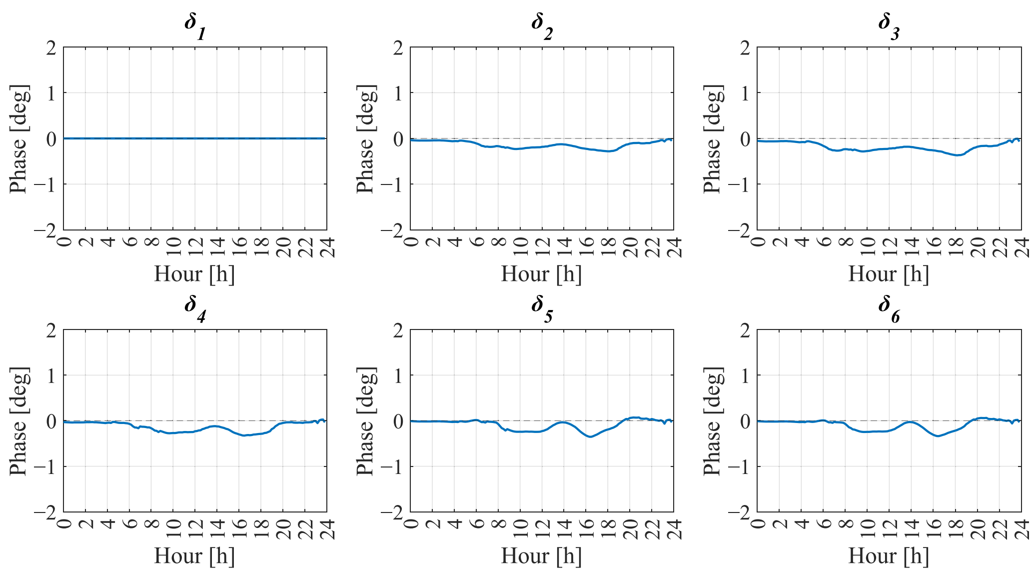

Fig. 24. "Full" EMS results – Voltage phases trends at nodes 1, 2, 3, 4, 5 and 6 – Base scenario – EMS 2.

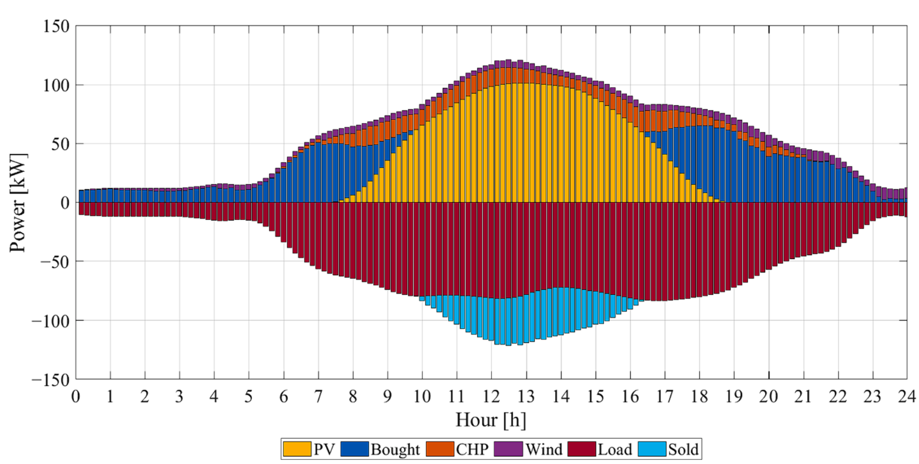

Fig. 25. "Full" EMS results – Active power – BESS out of service – EMS 1.

transformer is always positive, since for the whole day there is always the need of purchasing active energy. The flow between node 2 and node 3 is still always positive too, due to the large load installed at node 3. In this scenario, the active power flow $P_{3,4}$ is always negative, meaning that it is directed towards node 3. $P_{4,5}$ is negative during the central hours of day, when the production of the PV unit at node 5 is high and so the power flow is directed towards node 3; during the late night it becomes positive to feed the load at node 6 and to charge the BESS at node 5. $P_{5,6}$ is always positive as in the previous results, because either the BESS or the PV at node 5 are injecting active power. $P_{6,2}$ is negative for the whole day so, differently from the previous scenario, in order to limit the voltage deviation active power comes directly also from the transformer to satisfy the load at node 6.

Reactive power flows follow more or less the same trend, with the exception of $Q_{5,6}$ that takes much more limited values, if compared to the previous scenario, and of $Q_{3,4}$ that is reduced when the voltage deviation at each node is minimized. $Q_{4,5}$ is slightly modified, too. $Q_{1,2}$ is no longer equal to 0 but becomes positive during the hours in which there is the need of purchasing reactive energy from the network to support the voltage.

Fig. 23 and Fig. 24 finally report the trends of voltage modules and phases at each node. Voltage modules are now much closer to 1, if compared to the previous scenario. The lowest voltage is reached at node 3, where a large load is installed. At node 6 the voltage drop is more visible that at other nodes, due to the presence of another load. For all the nodes, the voltage drop is anyway reduced if compared to the results of the EMS minimizing only the operating costs.

Voltage phases are always very close to 0 [deg], thus laying in an acceptable interval.

3.4.3. BESS impact on MG operations

This subsubsection has the aim of analysing the impact of the BESS on the MG operation, considering a possible scenario in which BESS is out of service for maintenance reasons. The RES production is considered equal to the one in the Base Scenario.

3.4.3.1. Minimization of operating costs of the MG. The optimal active power dispatching results relevant to the objective function formulation taking into account only the operating costs of the MG, with the BESS out of service, are shown in Fig. 25. It is evident that during the night and the early morning, power is withdrawn from the external network just to meet the load. During the central hours of the day, the large PV production is used to satisfy the demand and the excess power is sold to the network. Again, during the evening, the external network has to provide the power needed to satisfy the load, in order to meet the demand, since WTs and CHP are not able by their own to provide the needed active power. Comparing Fig. 10 and Fig. 25, it is evident that the lack of the BESS does not allow to store energy coming from the distribution network during off-peak hours or from the PV during the central hours of the day, leading to a possible increase of operating costs. Curtailment is not applied to RES generators.

The ON/OFF results for DER units and for the exchange with the external network are reported in Fig. 26.

Reactive power dispatchment is not influenced by the unavailability of the BESS, since even in the base scenario it is not providing reactive power.

Looking at the voltage modules' profiles, shown in Fig. 27, it can be noted that they all lay within acceptable ranges, close to 1 [p.u.]. Overvoltages are evident during the central hours of the day due to the large PV production. Undervoltages can be found during early morning and the evening, when generation is close to 0 and almost all the power to satisfy the demand is withdrawn from the network.

Active power flows are reported in Fig. 28. It can be seen that the active power flow between busses 1 and 2, coinciding with the power exchanged with the external network, is positive during the morning and the evening, meaning that power has to be withdrawn from the external network, and is negative during the central hours of the day, when the surplus RES production is exported. The PV plant installed at bus 5 is a large plant, therefore power flows from its bus towards busses with load and towards the external network: in fact, $P_{5,6}$ and $P_{6,2}$ are positive and $P_{4,5}$ and $P_{3,4}$ are negative. The difference between $P_{4,5}$ and $P_{3,4}$ is given by the WT production, while the difference between $P_{3,4}$ and $P_{2,3}$ is given by the balance at node 3 between the local PV unit, CHP unit and load.

Reactive power flows are not modified since the unavailability of the BESS since even in the base scenario it is not providing reactive power.

3.4.3.2. Minimization of MG costs + Minimization of voltage deviation. The optimal active power dispatching results are presented in Fig. 29 and Fig. 30. From Fig. 30 it is possible to note that the PV plant at bus 5 undergoes curtailment during the central hours of the day in order to avoid overvoltages. Consequently, along with the absence of the BESS, for large part of the day power has to be withdrawn from the external network. ON/OFF dispatching statuses are presented in Fig. 31.

As in the previous subscenario, reactive power dispatching is not affected by the unavailability of the BESS.

Voltage amplitude trends are depicted in Fig. 32. The unavailability of the BESS is detrimental for the voltage support capacity of the MG: in

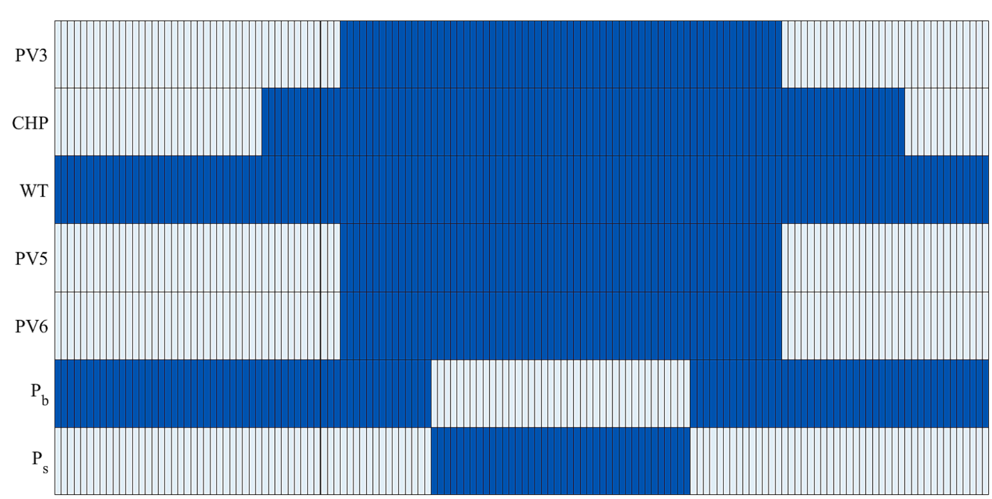

Fig. 26. "Full" EMS results – ON/OFF status of the units and of the network. Blue means that in that time interval the unit is ON or that the relevant exchange is different from 0, whilst white means that in that interval the unit is OFF or the relevant exchange is equal to 0 – BESS out of service – EMS 1. (For interpretation of the references to colour in this figure legend, the reader is referred to the web version of this article.)

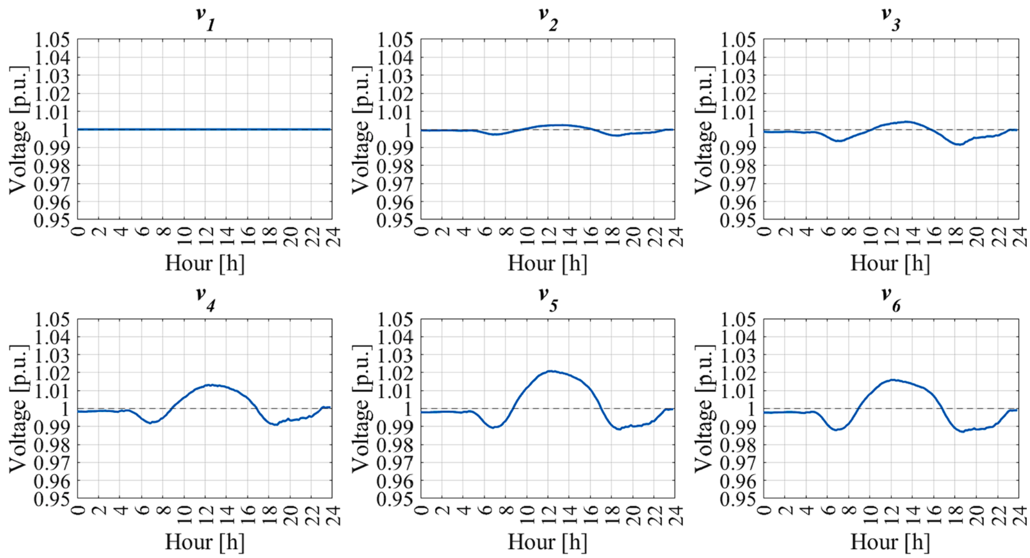

Fig. 27. “Full” EMS results – Voltage amplitudes at nodes 1,2,3,4,5 and 6 – BESS out of service – EMS 1.

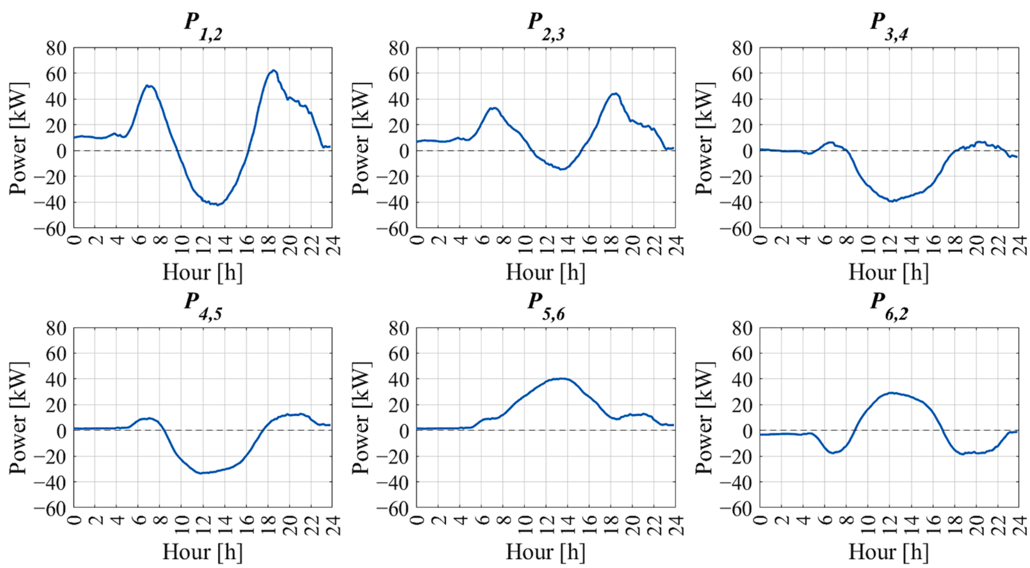

Fig. 28. “Full” EMS results – Active power flows on lines – BESS out of service – EMS 1.

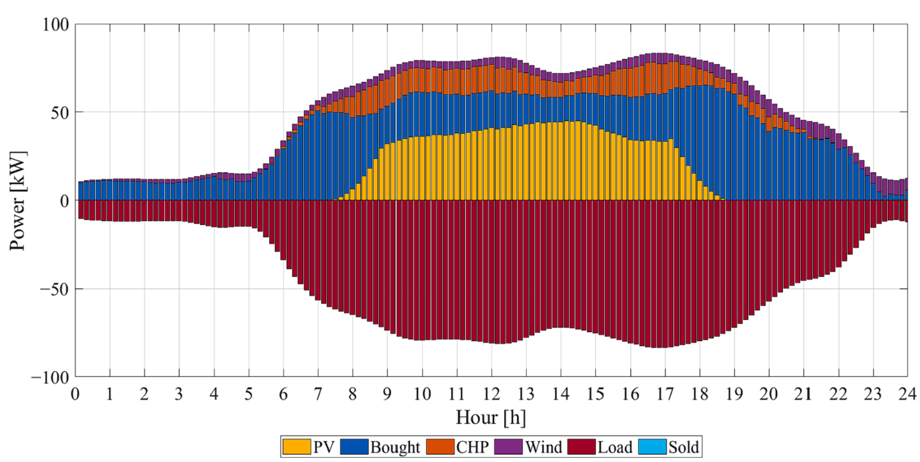

Fig. 29. “Full” EMS results – Active power – BESS out of service – EMS 2.

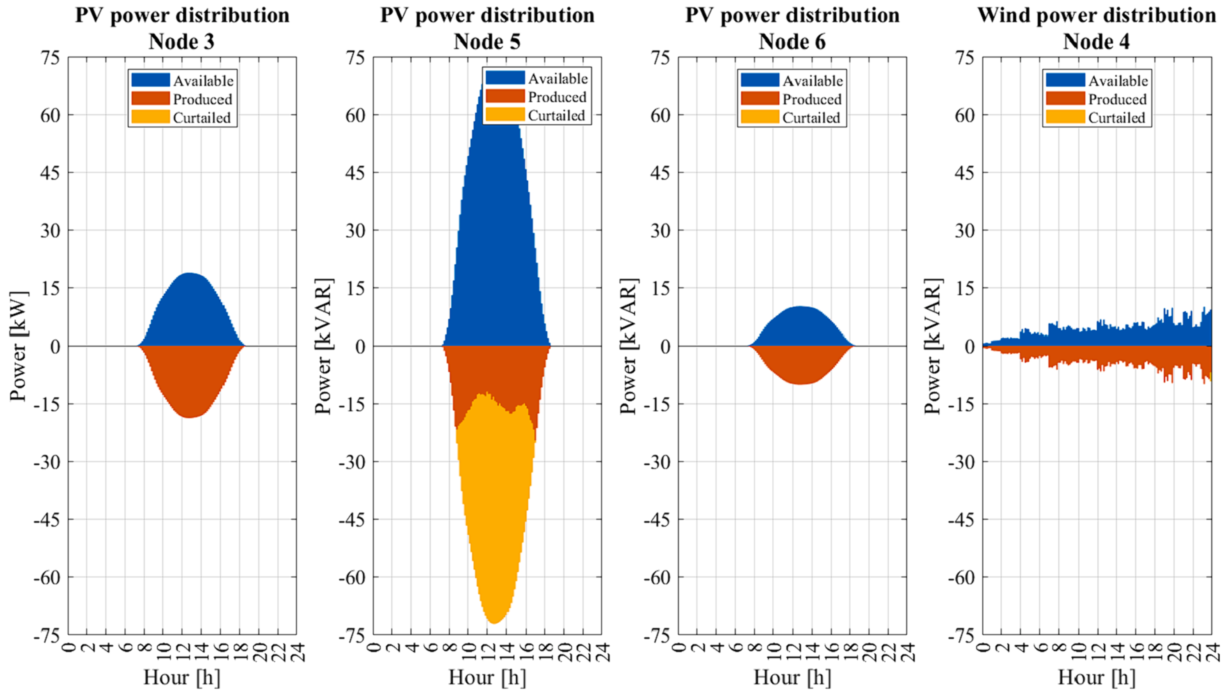

Fig. 30. "Full" EMS results – RES power distribution – BESS out of service – EMS 2 – In the positive direction of the vertical axis, the available power is reported. In the negative direction, the actual production of the sources and the curtailed power are reported, for each time interval. Negative values are used only for a comparison, being physically meaningless.

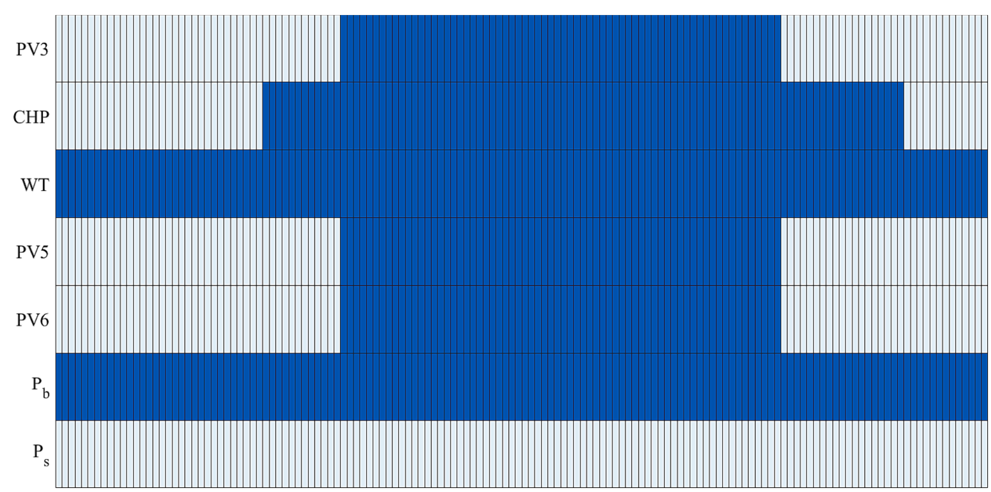

Fig. 31. "Full" EMS results – ON/OFF status of the units and of the network. Blue means that in that time interval the unit is ON or that the relevant exchange is different from 0, whilst white means that in that interval the unit is OFF or the relevant exchange is equal to 0 – BESS out of service – EMS 2. (For interpretation of the references to colour in this figure legend, the reader is referred to the web version of this article.)

fact, it is evident that around 7 AM and 7 PM undervoltage conditions occur, due to the reduced RES production and to the fact that almost all the power to satisfy the demand is withdrawn from the network.

Active power flows are reported in Fig. 33. $P_{1,2}$ and $P_{2,3}$ are always positive, since for the whole day there is the need of purchasing energy from the network. $P_{4,5}$ and $P_{5,6}$ are respectively negative and positive during the central hours of the day, to provide the production of the PV plant at bus 5 to busses 6 and 3, where the loads are located. During the early morning and the evening, power is provided to the load at bus 6 both directly from bus 2 (i.e., when $P_{6,2}$ is negative) and through busses 3–4-5 ($P_{2,3}$, $P_{3,4}$, $P_{4,5}$, $P_{5,6}$ are simultaneously positive). Reactive power flows are not modified since the unavailability of the BESS since even in the base scenario it is not providing reactive power.

3.4.4. *RES penetration impact on MG operations*

This subsubsection provides the results of a sensitivity analysis carried out to investigate the effect of RES penetration on the operations of the MG. In particular, the available energy for the PV plants at busses 3 and 6 and for the WT plant at bus 4 is doubled if compared to the base scenario presented in 3.4.1 and 3.4.2. Since the optimal design procedure is considered to be already performed, the production of the PV power plant at node 5 is not increased since it could lead to the violation of cables' capacity. BESS is considered to be in service.

3.4.4.1. Minimization of MG costs. The results of the EMS for active power dispatching are presented in Fig. 34. As it can be noted, the increased RES availability allows to sell some energy to the external network during the central hours of the day, along with the charging of

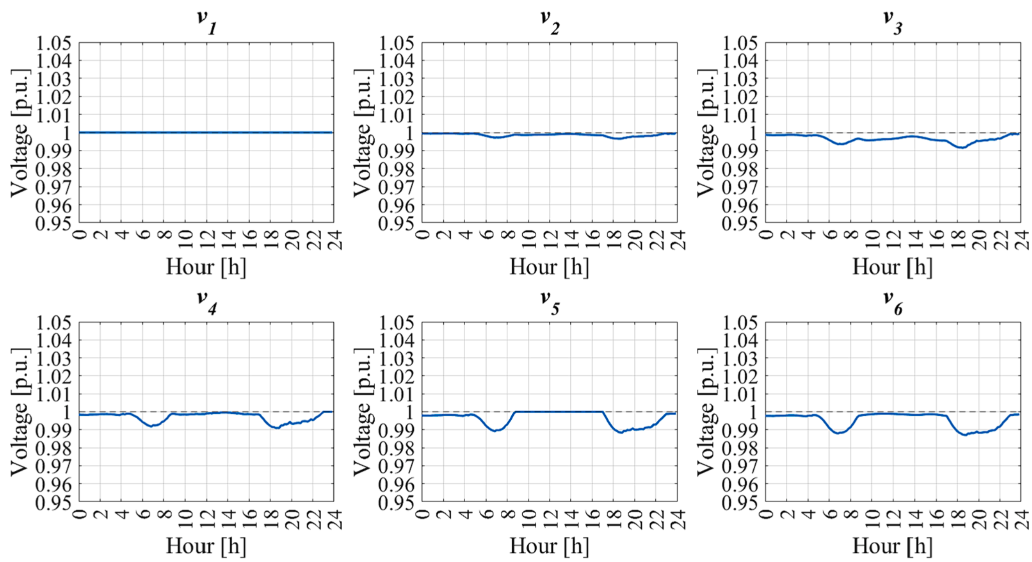

Fig. 32. "Full" EMS results – Active power flows on lines – BESS out of service – EMS 2.

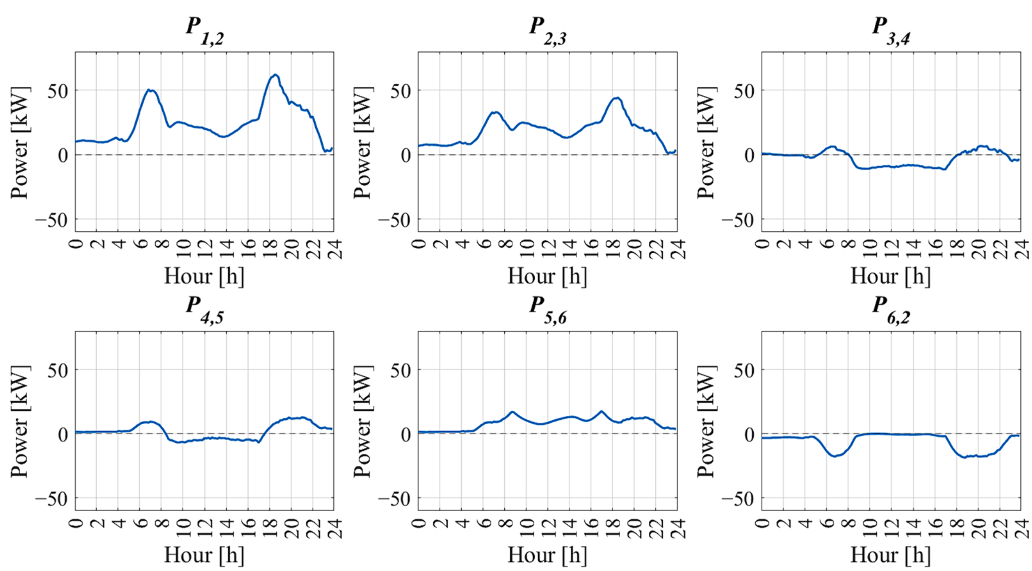

Fig. 33. "Full" EMS results – Active power flows on lines – BESS out of service – EMS 2.

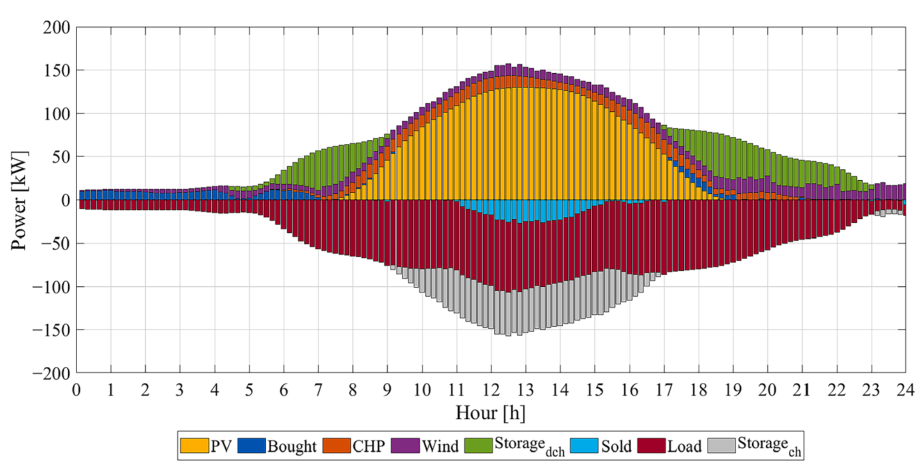

Fig. 34. "Full" EMS results – Active power – Increased RES penetration – EMS 1.

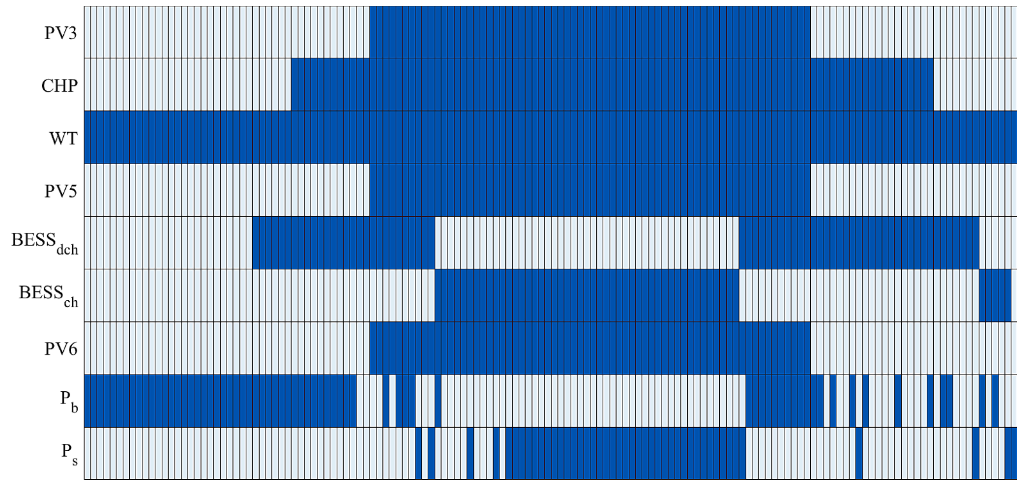

Fig. 35. "Full" EMS results – ON/OFF status of the units and of the network. Blue means that in that time interval the unit is ON or that the relevant exchange is different from 0, whilst white means that in that interval the unit is OFF or the relevant exchange is equal to 0 – Increased RES penetration – EMS 1. (For interpretation of the references to colour in this figure legend, the reader is referred to the web version of this article.)

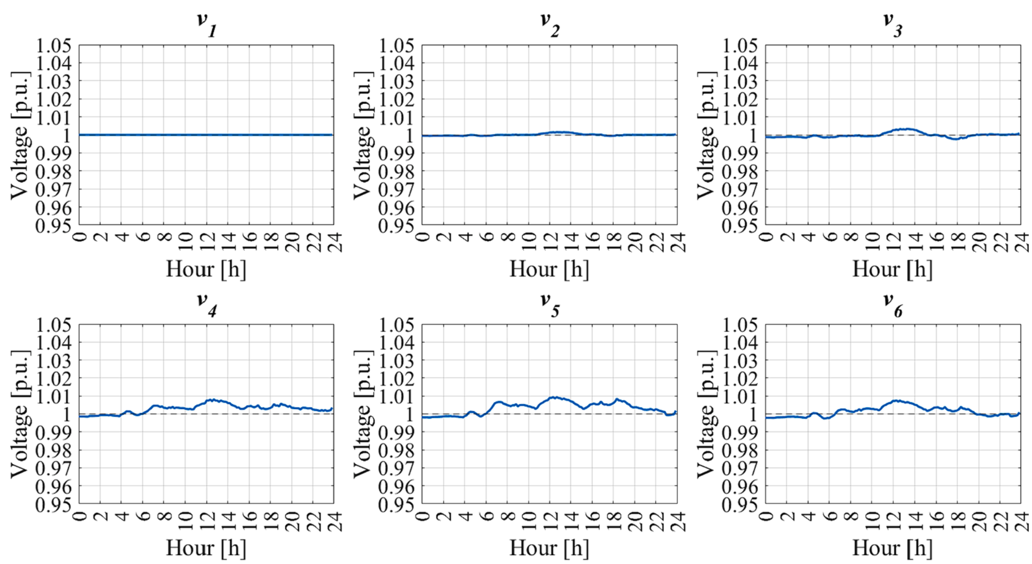

Fig. 36. "Full" EMS results – Voltage modules at nodes 1,2,3,4,5 and 6 – Increased RES penetration – EMS 1.

the BESS to increase the self-consumption of the facility. Besides, the increased WT production, combined with the discharging of the BESS, allows to avoid the purchase of energy from the external network during the evening: energy is purchased only during the early morning when the price of electricity is low, just to satisfy the demand. Besides, during the last time intervals, the BESS is charged, avoiding curtailment of the WT source.

The ON/OFF status of the DER units and of the exchange with the network is reported in Fig. 35.

Voltage amplitudes at the MG busses are presented in Fig. 36. The increased RES penetration allows to smooth the undervoltage issues that were evident in the base scenario. On the contrary, overvoltage trends become more evident during the central hours of the day at all the nodes, due to the higher active power injection by RES generators.

Active power flows, reported in Fig. 37, are strongly modified, given the surplus of RES energy during the central hours of the day: in fact, if compared to the base scenario, the active power flow from node 1 to node 2 (i.e., the exchange with the external network) is still positive but closer to 0 during the early morning and the late evening, when there is the need of withdrawing energy from the network, whilst it becomes negative during the central hours of the day, when selling the surplus of RES production. The same trend can be highlighted for the active power flow from bus 2 to bus 3. Besides, if compared to the base scenario, the active power flows $P_{3,4}$ and $P_{4,5}$ become negative or at least 0 during the early morning (around 4 AM), since the battery is no more charged at that time. For the same reason, $P_{6,2}$ becomes closer to 0 in the same time intervals.

3.4.4.2. Minimization of MG costs + Minimization of voltage deviation. The results referred to the scenario with increased RES penetration, taking into account in the objective function both the minimisation of costs and the minimisation of the voltage deviation from the rated values are shown below.

The active power dispatching results are reported in Fig. 38. Compared to the scenario proposed in 3.4.4.1, the need for minimization of voltage deviation at the busses introduces substantial changes in the dispatching of the units. First, as it can be noted also from Fig. 39, the PV plant at node 5 undergoes curtailment during basically the whole day, to avoid overvoltage issues. In order to support the voltage, the BESS discharges from midnight until around 9 AM, when it reaches the minimum

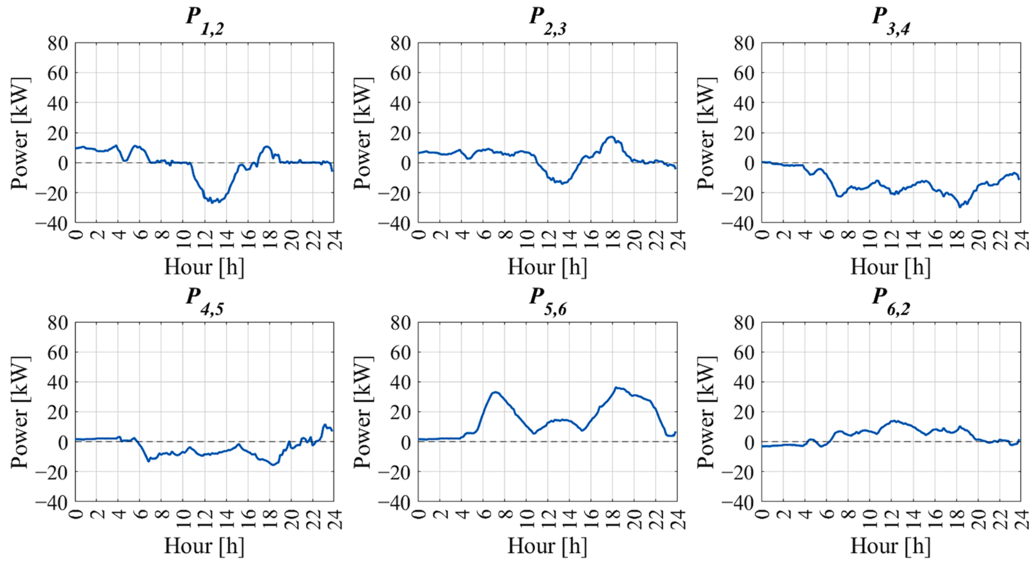

Fig. 37. "Full" EMS results – Active power flows on lines – Increased RES penetration – EMS 1.

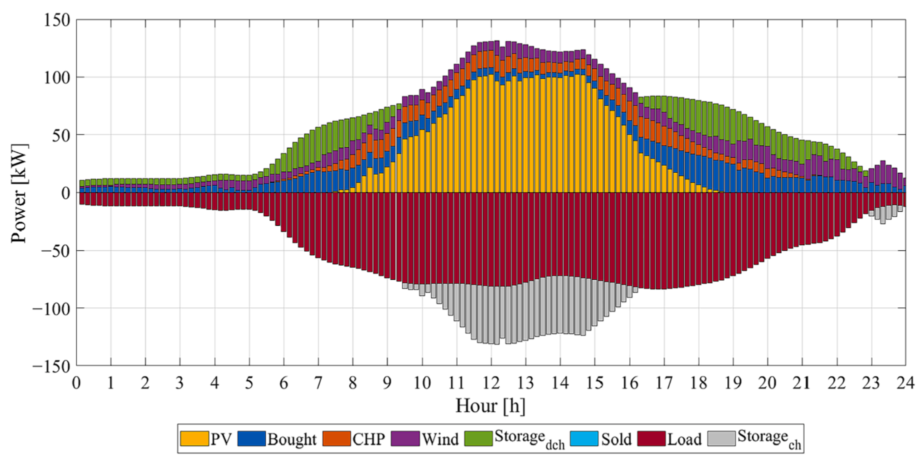

Fig. 38. "Full" EMS results – Active power – Increased RES penetration – EMS 2.

state of charge. Then, the BESS is charged exploiting surplus PV energy, trying to reduce the curtailment of the PV plant at node 5 until 4PM, when it discharges again to support the voltage. Finally, during the late evening it is charged again. Active power is withdrawn from the external network for the whole day, again to support voltage. The ON/OFF status of the DER units and of the exchange with the network is shown in Fig. 40.

Voltage amplitude profiles at the MG busses are reported in Fig. 41. Due to the formulation of the objective function, voltage modules are very close to 0 at all busses. The only significant undervoltage behaviours can be seen at busses 3 and 6 where the loads are installed and at bus 5 where the BESS is installed, for the hours in which it works in charging mode.

Finally, the active power flows are reported in Fig. 42. If compared to the results shown in 3.4.4.2, it can be noted that the flow $P_{1,2}$ is always positive, meaning that there is no sale of electricity to the network. It is interesting to note that $P_{5,6}$ assumes values close to 0 during the central hours of the day, meaning that all the power produced by the local PV plant is absorbed by the BESS.

3.4.5. Comparison of energy and economic indicators

In this part, a comparison between the results obtained with the two formulations of the objective function will be presented, discussing the main differences and the main advantages of each one. Table 4 reports the main energy and economic quantities that have been obtained. The three considered scenarios are reported: the Base Scenario, the scenario with the BESS out of service and the scenario with increased RES penetration. "EMS 1" refers to the EMS's results considering only the minimization of costs, whilst "EMS 2" refers to the results of the EMS that minimizes both the costs and the voltage deviation.

Considering the two EMS formulation applied to the Base Scenario, NCs undergo a 42% increase, if the voltage deviation has also to be minimized. In this case, BESS energy exchange with the MG is almost the same, with a slight reduction: together with the fact that the charging phase is concentrated only during the central hours of the day, the behaviour of the BESS is optimized to keep the nodal voltages close to the rated value. For the same reason, PV undergoes curtailment: the amount of curtailed energy is equal to the 10% of the overall available one. For WT curtailment is basically negligible. For the purpose of voltage deviation minimization, a larger amount of active energy has to be withdrawn from the external network, with a 24.5% increase. As previously explained, also the reactive energy provision is distributed differently among the different sources.

Since the nodal voltages are already close to 1 in the results of "EMS 1", with the largest deviation corresponding to a module of about 0.98 [p.u.], the increase in NCs that arises in "EMS 2" may not be acceptable.

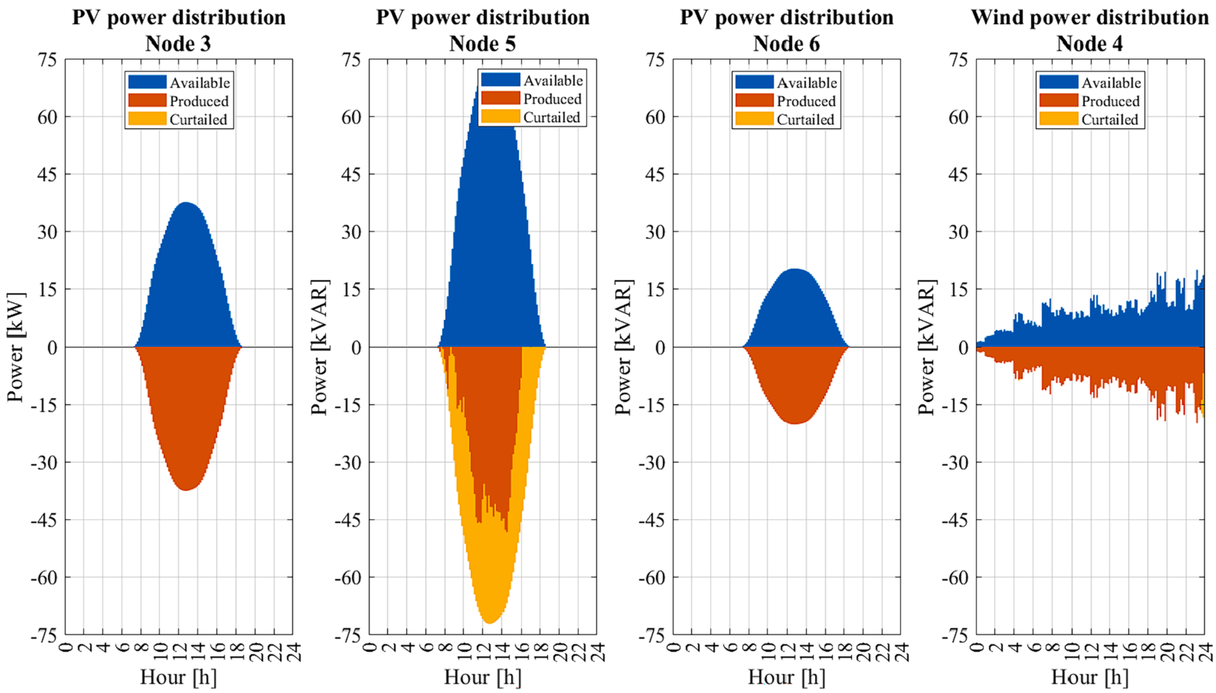

Fig. 39. "Full" EMS results – RES power distribution – Increased RES penetration – EMS 2 – In the positive direction of the vertical axis, the available power is reported. In the negative direction, the actual production of the sources and the curtailed power are reported, for each time interval. Negative values are used only for a comparison, being physically meaningless.

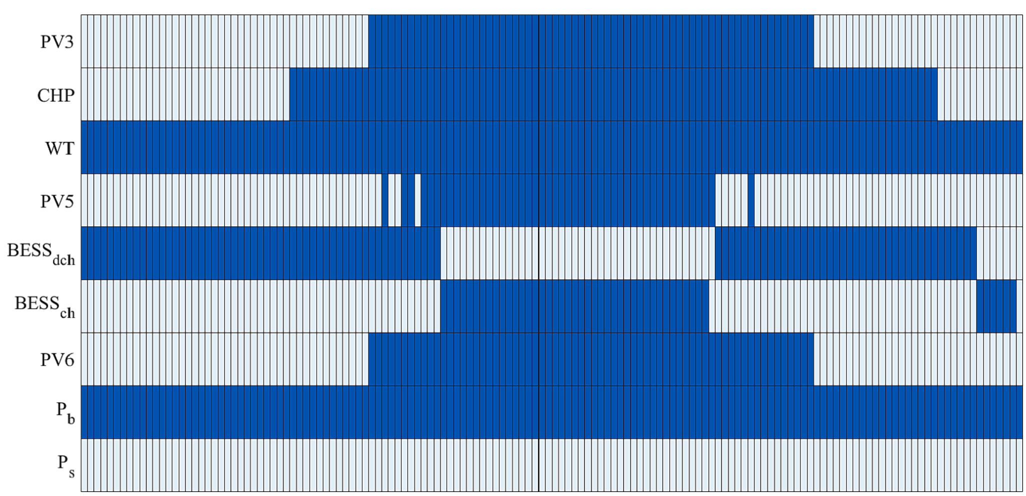

Fig. 40. "Full" EMS results – ON/OFF status of the units and of the network. Blue means that in that time interval the unit is ON or that the relevant exchange is different from 0, whilst white means that in that interval the unit is OFF or the relevant exchange is equal to 0 – Increased RES penetration – EMS 2. (For interpretation of the references to colour in this figure legend, the reader is referred to the web version of this article.)

Besides, in "EMS 2" PV source is not fully exploited due to curtailment. Therefore, in small MGs with short distances between busses, the first formulation of the objective function is effective enough in optimizing the operations of the facility, both from a technical and an economic point of view.

Comparing the Base Scenario with the scenario in which the BESS is out of service, it can be noted that when the optimal dispatching of the sources is aimed at minimizing the operating costs, the RES production is sold when in excess and active power is withdrawn from the external network when the generation of the MG is not able to meet the demand. Operating costs are increased of 39% if compared to the Base Scenario with the same objective.

When the objective function takes also into account the minimization of voltage deviation, massive curtailment has to be applied to the PV

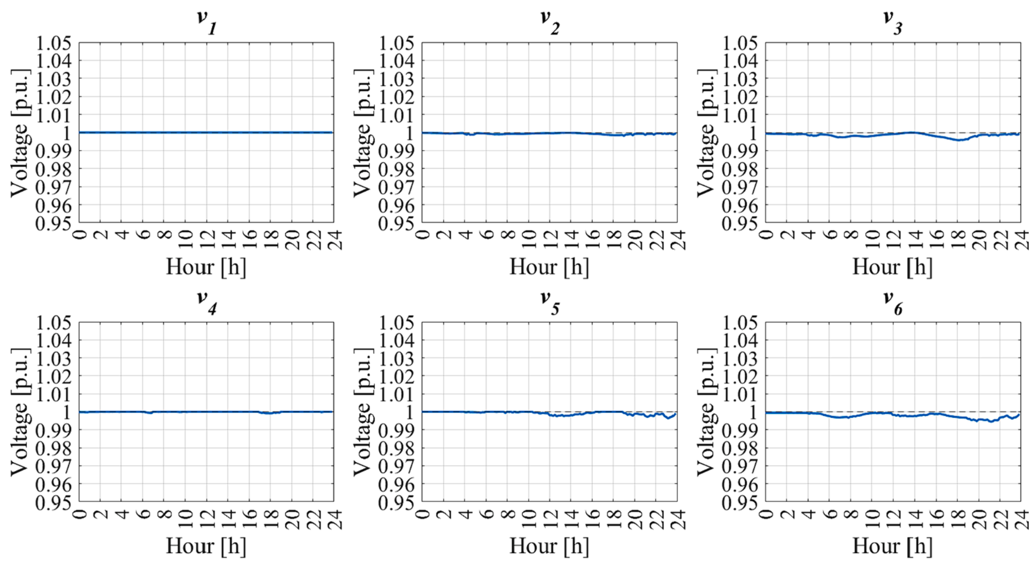

Fig. 41. "Full" EMS results – Voltage modules at nodes 1,2,3,4,5 and 6 – Increased RES penetration – EMS 2.

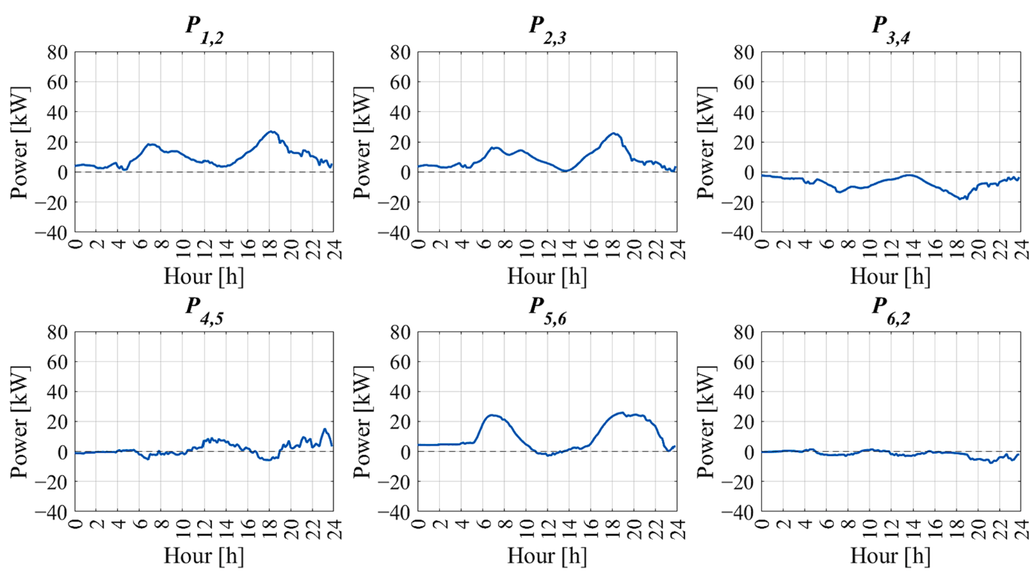

Fig. 42. "Full" EMS results – Active power flows on lines – EMS 2.

source at node 5, up to almost half of the available energy. In order to keep the voltage voltages close to the rated values and due to the consequent curtailment, a lot of energy has to be withdrawn from the external network, thus significantly increasing the operating costs (+62% if compared to the base scenario with the same objective).

Considering the third scenario, where the RES penetration is increased, with the minimization uniquely of the operating costs, it can be seen that no curtailment is applied to RES generators. Besides, less energy is bought from the external network, if compared to same EMS formulation in the other two scenario, and some energy is even sold during surplus periods. Therefore, operating costs are reduced of 88% if compared to the Base Scenario. The BESS is more exploited in order to store excess RES power and use it when needed. If the minimization of voltage deviation is considered, the operating costs are higher since more energy has to be purchased from the external network. Curtailment is again applied both to the PV and WT generators but less than in the scenario with BESS out of service.

Indeed, the presence of the BESS is beneficial to avoid curtailment and to keep the voltage deviation close to 1. In scenario with increased RES penetration, the increase of operating costs to minimize voltage deviation is massive (8 times more than in the same scenario with the minimization of costs only), therefore other voltage support measures may be investigated. In the other scenarios, instead, the operating costs' increase to minimize voltage deviation is more limited if compared to the subscenario considering the minimization of costs only.

4. Conclusions

The purpose of this paper was to develop an EMS for the efficient management of a polygenerative MG connected to the external distribution network, composed of different busses at which RES generators, a CHP unit, a BESS and several loads are installed. Two objective function's formulations were provided, one minimizing the operating costs of the MG, associated with the active and reactive energy exchange with the external network and with the curtailment of RES generation, and one minimizing both the aforementioned operating costs and the deviation of the nodal voltages from the rated value.

The proposed approach represents a significant contribution offering

Table 4
Main energy and economic results of the two EMSs for the three scenarios.

	[–]	Base Scenario		BESS out of service		Increased RES penetration	
		EMS 1	EMS 2	EMS 1	EMS 2	EMS 1	EMS 2
PV active energy generation	[kWh]	698.56	625.48	698.56	360.99	898.14	632.19
PV active energy curtailment	[kWh]	0	73.08	0	337.56	0	265.95
PV reactive energy generation	[kVARh]	236.83	244.33	236.83	244.33	193.55	277.77
PV reactive energy absorption	[kVARh]	0	0	0	0	0	0
WT active energy generation	[kWh]	111.07	110.67	111.07	110.67	222.14	219.53
WT active energy curtailment	[kWh]	0	0.40	0	0.40	0	2.61
WT reactive energy generation	[kVARh]	46.36	38.87	46.36	38.87	89.64	3.29
WT reactive energy absorption	[kVARh]	0	0	0	0	0	0
CHP active energy generation	[kWh]	164.49	164.49	164.49	164.49	164.49	164.49
CHP reactive energy generation	[kVARh]	317.55	317.55	317.55	317.55	317.55	302.39
CHP reactive energy absorption	[kVARh]	0	0	0	0	0	0
BESS charged active energy	[kWh]	297.02	287.38	–	–	315.87	249.99
BESS discharged active energy	[kWh]	268.06	259.36	–	–	285.08	225.61
BESS reactive energy generation	[kVARh]	0	0	–	–	0	0
BESS reactive energy absorption	[kVARh]	0	0	–	–	0	0
Bought active energy	[kWh]	295.35	367.74	450.21	604.21	72.65	248.53
Sold active energy	[kWh]	0	0	183.96	0	86.26	0
Bought reactive energy	[kVARh]	0	2.40	0	2.40	0	17.29
Sold reactive energy	[kVARh]	0	0	0	0	0	0
NCs	[€]	79.73	113.10	111.05	182.51	9.47	76.21

a coupled optimization of both active and reactive power flows, thanks to the implementation within the mathematical model of OPF equations, along with a detailed characterization of the cables and connections.

Furthermore, the paper explores the potential computational benefits that derive from the linearization of OPF equations that conventionally involve non-linearities. To this aim, a simplified MG made of three nodes was preliminarily considered in order to assess the accuracy of the results of an EMS containing linearized OPF equations, if compared to the results of an EMS with non-linear ones. A sensitivity analysis was carried out, varying the length of the connecting lines: as a result, this analysis endorsed the linearization of the OPF equations, to be then applied in the EMS applied to the "full" polygenerative MG.

A discussion about the results of the "full" EMSs was eventually carried out, showing that the minimization of voltage deviation induces an increase of the operating costs, related both to an increase of the costs related to the purchase of active energy from the external network and to an increase of the curtailments costs for PV and WT. This also causes a change in the distribution of the internodal active and reactive power flows. Anyway, from a technical point of view, it is preferrable to keep nodal voltages close to the rated value.

Additional scenarios were investigated to assess the impact of BESS unavailability and of increased RES penetration on the operation of the MG: the former scenario showed that the BESS has an important role in voltage support, while the latter proves that increased RES penetration leads to a reduction of the operating costs of the facility.

In conclusion, this work advances the understanding and practical implementation of EMSs for polygenerative MGs, contributing to the ongoing efforts to enhance the reliability, efficiency, and sustainability of power systems. The insights gained from this research can guide future developments in the field of MG optimization, paving the way for future studies that may include the evaluation of the impact of fleet of EVs on the MG operations and the possible advantages that may derive from the installation of electrolysers and hydrogen fuel cells within the facility.

CRediT authorship contribution statement

Matteo Fresia: Writing – original draft, Software, Methodology, Conceptualization. **Laura Bordo:** Writing – original draft, Software, Methodology. **Federico Delfino:** Supervision. **Stefano Bracco:** Writing – review & editing, Methodology, Conceptualization.

Declaration of competing interest

The authors declare that they have no known competing financial interests or personal relationships that could have appeared to influence the work reported in this paper.

Data availability

The data that has been used is confidential.

References

[1] *Fit for 55*. Available: https://europa.eu/!7G9njr.
[2] Franco A, Salza P. Strategies for optimal penetration of intermittent renewables in complex energy systems based on techno-operational objectives. Renew Energy 2011;36(2):743–53.
[3] Mladenov V, Chobanov V, Georgiev A. Impact of renewable energy sources on power system flexibility requirements. Energies 2021;14(10):2813.
[4] Denholm P, Hand M. Grid flexibility and storage required to achieve very high penetration of variable renewable electricity. Energy Policy 2011;39(3):1817–30.
[5] Oudalov A, Cherkaoui R, Beguin A. Sizing and optimal operation of battery energy storage system for peak shaving application. In: 2007 IEEE Lausanne Power Tech. IEEE; 2007. p. 621–5.
[6] Conejo AJ, Cheng Y, Zhang N, Kang C. Long-term coordination of transmission and storage to integrate wind power. CSEE J Power Energy Syst 2017;3(1):36–43.
[7] Fresia M, et al. A techno-economic assessment to define inertia needs of the Italian transmission network in the 2030 energy scenario. IEEE Trans Power Syst 2023:1–12.
[8] Hatziargyriou N, Asano H, Iravani R, Marnay C. Microgrids. IEEE Power Energ Mag 2007;5(4):78–94.
[9] Muhtadi A, Pandit D, Nguyen N, Mitra J. Distributed energy resources based microgrid: Review of architecture, control, and reliability. IEEE Trans Ind Appl 2021;57(3):2223–35.
[10] Wang X, Guerrero JM, Blaabjerg F, Chen Z. A review of power electronics based microgrids. Internat J Power Electron 2012;12(1):181–92.
[11] Lasseter R. Smart distribution: Coupled microgrids. Proc IEEE 2011;99(6):1074–82.
[12] Rafique SF, Jianhua Z. Energy management system, generation and demand predictors: a review. IET Gener Transm Distrib 2018;12(3):519–30.
[13] Thakar S, Vijay AS, Doolla S. Effect of P-Q limits on microgrid reconfiguration: A capability curve perspective. IEEE Trans Sustainable Energy 2020;11(3):2040–8.
[14] Abdi H, Beigvand SD, La Scala M. A review of optimal power flow studies applied to smart grids and microgrids. Renew Sustain Energy Rev 2017;71:742–66.
[15] Arkhangelski J, Mahamadou A-T, Lefebvre G. Data forecasting for optimized urban microgrid energy management. In: 2019 IEEE International Conference on Environment and Electrical Engineering and 2019 IEEE Industrial and Commercial Power Systems Europe (EEEIC/I&CPS Europe). IEEE; 2019. p. 1–6.
[16] Arkhangelski J, Abdou-Tankari M, Lefebvre G. Day-ahead optimal power flow for efficient energy management of urban microgrid. IEEE Trans Ind Appl 2021;57(2):1285–93.
[17] Bracco S, Fresia M. Energy management system for the optimal operation of a grid-connected building with renewables and an electric delivery vehicle. In: IEEE

EUROCON 2023-20th International Conference on Smart Technologies. IEEE; 2023. p. 472–7.

[18] Fresia M, Bracco S. Electric vehicle fleet management for a prosumer building with renewable generation. Energies 2023;16(20):7213.

[19] Azuara-Grande LS, Arnaltes S, Alonso-Martinez J, Rodriguez-Amenedo JL. Comparison of two energy management system strategies for real-time operation of isolated hybrid microgrids. Energies 2021;14(20):6770.

[20] Tazvinga H, Zhu B, Xia X. Optimal power flow management for distributed energy resources with batteries. Energ Conver Manage 2015;102:104–10.

[21] Merabet A, Al-Durra A, El-Saadany E. Energy management system for optimal cost and storage utilization of renewable hybrid energy microgrid. Energ Conver Manage 2022;252:115116.

[22] Roy A, et al. A combined optimization of the sizing and the energy management of an industrial multi-energy microgrid: Application to a harbour area. Energ Conver Manage 2021;12:100107.

[23] Et-Taoussi M, Ouadi H, Chakir HE. Hybrid optimal management of active and reactive power flow in a smart microgrid with photovoltaic generation. Microsyst Technol 2019;25:4077–90.

[24] Piazza G, Bracco S, Delfino F, Siri S. Optimal design of electric mobility services for a Local Energy Community. Sustainable Energy Grids Networks 2021;26:100440.

[25] Dong W, et al. Stochastic optimal scheduling strategy for a campus-isolated microgrid energy management system considering dependencies. Energ Conver Manage 2023;292:117341.

[26] Thai C, Brouwer J. Decarbonizing a solar PV and gas turbine microgrid with hydrogen and batteries. Energ Conver Manage 2023;292:117391.

[27] Bianco G, Delfino F, Ferro G, Robba M, Rossi M. A hierarchical Building Management System for temperature's optimal control and electric vehicles' integration. Energy Convers Manage: X 2023;17:100339.

[28] Bracco S, Delfino F, Pampararo F, Robba M, Rossi M. A system of systems model for the control of the university of Genoa Smart Polygeneration Microgrid. In: 2012 7th International Conference on System of Systems Engineering (SoSE); 2012. p. 7–12.

[29] Bracco S, Delfino F, Pampararo F, Robba M, Rossi M. Planning and management of sustainable microgrids: The test-bed facilities at the University of Genoa. Africon 2013;2013:1–5.

[30] Bahlawan H, Castorino GAM, Losi E, Manservigi L, Spina PR, Venturini M. Optimal management with demand response program for a multi-generation energy system. Energy Convers. Manage. X 2022;16:100311.

[31] Nusair K, Alasali F. Optimal power flow management system for a power network with stochastic renewable energy resources using. Golden Ratio Optim. Method 2020;13(14):3671.

[32] Shezan SA, et al. Effective dispatch strategies assortment according to the effect of the operation for an islanded hybrid microgrid. Energy Convers. Manage. X 2022; 14:100192.

[33] Y.R.O, J.J, Chakraborty AK, Guerrero JM. Stochastic optimal power flow in islanded DC microgrids with correlated load and solar PV uncertainties. Appl Energy 2022;307:118090.

[34] Ayele GT, Mabrouk MT, Haurant P, Laumert B, Lacarrière B. Optimal heat and electric power flows in the presence of intermittent renewable source, heat storage and variable grid electricity tariff. Energ Conver Manage 2021;243:114430.

[35] Liang R-H, Wang J-C, Chen Y-T, Tseng W-T. An enhanced firefly algorithm to multi-objective optimal active/reactive power dispatch with uncertainties consideration. Int J Electr Power Energy Syst 2015;64:1088–97.

[36] Gabash A, Li P. Active-reactive optimal power flow for low-voltage networks with photovoltaic distributed generation. In: 2012 IEEE international energy conference and exhibition (ENERGYCON). IEEE; 2012. p. 381–6.

[37] Mastromauro RA. Analysis of performances of single-phase PV transformer-less inverters for compliance with the new standards CEI 0–21and IEEE 1547–2018. In: 2023 IEEE 17th international conference on compatibility, power electronics and power engineering (CPE-POWERENG); 2023. p. 1–6.

[38] Šúri M, Huld T, Cebecauer T, Dunlop ED. Geographic aspects of photovoltaics in Europe: contribution of the PVGIS web site. IEEE J Selected Top Appl Earth Observ Remote Sens 2008;1(1):34–41.

[39] de Simón-Martín M, Bracco S, Piazza G, Pagnini LC, González-Martínez A, Delfino F. Application to real case studies. In: Levelized cost of energy in sustainable energy communities: a systematic approach for multi-vector energy systems. Cham: Springer International Publishing; 2022. p. 77–120.

[40] Lofberg J. YALMIP: A toolbox for modeling and optimization in MATLAB. In: 2004 IEEE international conference on robotics and automation (IEEE Cat. No. 04CH37508). IEEE; 2004. p. 284–9.

[41] L. Gurobi Optimization. (2023). Gurobi Optimizer Reference Manual. Available: https://www.gurobi.com.

[42] Wächter A, Biegler L. On the implementation of an interior-point filter line-search algorithm for large-scale nonlinear programming. Math Program 2006;106:25–57.

[43] Lavi Y, Apt J. Using PV inverters for voltage support at night can lower grid costs. Energy Rep 2022;8:6347–54.

[44] Talkington S, Grijalva S, Reno MJ, Azzolini JA. Solar PV inverter reactive power disaggregation and control setting estimation. IEEE Trans Power Syst 2022;37(6): 4773–84.